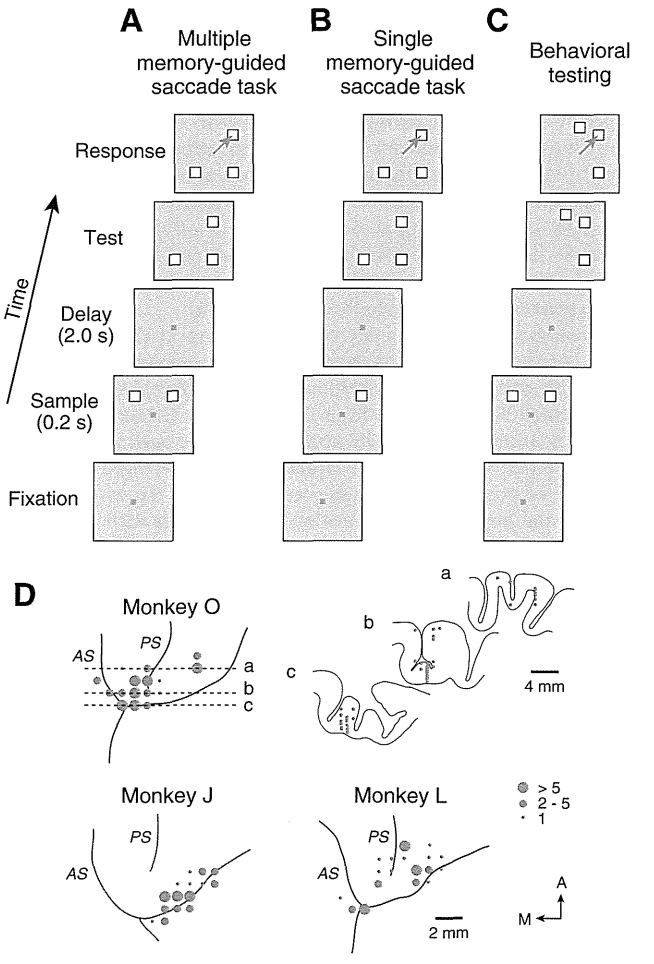

Figure 1. Behavioral paradigms and recording sites. ***A***, Sequence of events in the MMS task. Monkeys remembered two sample locations during the delay and made a saccade to one of three test stimuli presented at either sample location. Both the sample and test stimuli were chosen from four possible locations (cardinal or oblique locations). ***B***, In the SMS task, only one sample was presented. ***C***, For the behavioral experiment, test stimuli were chosen from eight possible locations. ***D***, Recording sites. The size of each circle indicates the number of recorded neurons. Coronal sections were shown only for Monkey O at the level indicated by broken lines. PS, Principal sulcus; AS, arcuate sulcus.

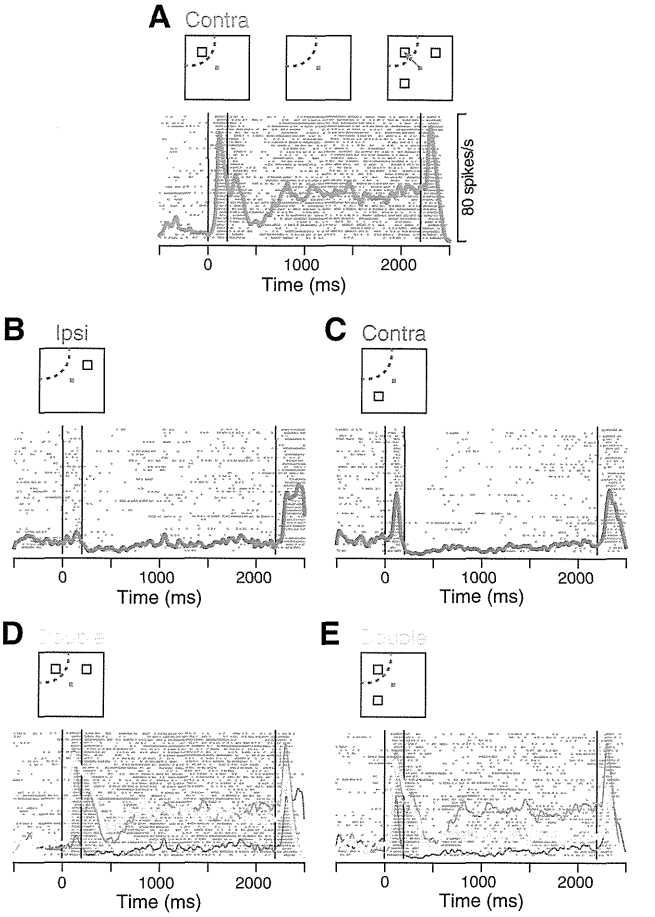

Figure 2. Activity of a representative neuron. ***A***, Activity in the SMS trials with a sample in the RF. From left to right, vertical lines indicate the onset and offset of the sample, and the onset of test stimuli. ***B***, ***C***, Activity in the SMS trials with a sample presented 90° away from the RF. ***D***, When two samples were presented across the left and right visual fields (green), the activity was similar to that for the single sample presented in the RF (red, the same data as in ***A***). ***E***, When two samples were presented within the same visual field (green), the neuron exhibited an intermediate response to those for each stimulus presented alone (red and blue traces, the same data as in ***A*** and ***C***).

Materials and Methods

Animal preparation. Experiments were conducted on three Japanese macaques (*Macaca fuscata*, 6–7 kg female, Monkeys J, L, and O). All animal protocols were approved by the Animal Care and Use Committee of Hokkaido University and were in accord with the Guide for the Care and Use of Laboratory Animals. The animal preparation procedure was described previously in detail (Tanaka, 2005). Briefly, a pair of head holders was implanted on the skull using titanium screws and dental acrylic under general isoflurane anesthesia. A coil of stainless steel wire was implanted under the conjunctiva. During subsequent training and experimental sessions, the monkey's head was secured to the primate chair, and eye positions were continuously recorded using the search coil technique (MEL-25; Enzanshi Kogyo). After training on behavioral tasks, a recording cylinder was installed over a small craniotomy, allowing electrode penetrations into the prearcuate PFC. Animals received analgesia after each surgery. The monkeys' water intake was controlled daily so that they were motivated to perform the tasks.

Visual stimuli and behavioral paradigms. Experiments were controlled by a Windows-based real-time data acquisition system (TEMPO; Reflective Computing). Visual stimuli were presented on a 24-inch cathode-ray tube monitor (60 Hz) positioned 38 cm from the eyes and subtending 64 × 44° of visual angle. Experiments were performed in a darkened booth. Each trial began with the appearance of a fixation point (FP, 0.5° red square) at the center of the screen. Monkeys were required to maintain fixation for >300 ms to proceed with the trial. Correct performance was reinforced with a drop of liquid reward at the end of each trial.

During recording sessions, we presented two memory-guided saccade tasks. In the multiple memory-guided saccade (MMS) task (see Fig. 1*A*), two sample (200 ms) and three test stimuli were presented 12° eccentrically across a 2 s delay (1° white squares). One test stimulus was presented at the same location as either sample (matched stimulus), whereas the others were presented elsewhere (nonmatched stimuli). The location of the matched stimulus was chosen randomly from the two sample locations so that the animals had to remember both locations. Monkeys were required to keep their eyes within 5° of the central FP during the sample and delay periods, then to make a saccade to the matched stimulus in response to the FP offset and the simultaneous appearance of test stimuli (<400 ms). As a control, we also presented the single memory-guided saccade (SMS) task with only one sample stimulus (see Fig. 1*B*). In all recording sessions, the deviation of eye position from the FP was much less than the window size (mean ± SD, 0.51 ± 0.11°, 0.50 ± 0.14°, and 0.64 ± 0.14°, for Monkeys J, L, and O, respectively). Both sample and test stimuli appeared either at four oblique (45°, 135°, 225°, or 315° measured from rightward) or four cardinal (0°, 90°, 180°, or 270°) polar angles. Different tasks were presented pseudo-randomly within a block that usually consisted of the SMS trials in four oblique and/or four cardinal (90°

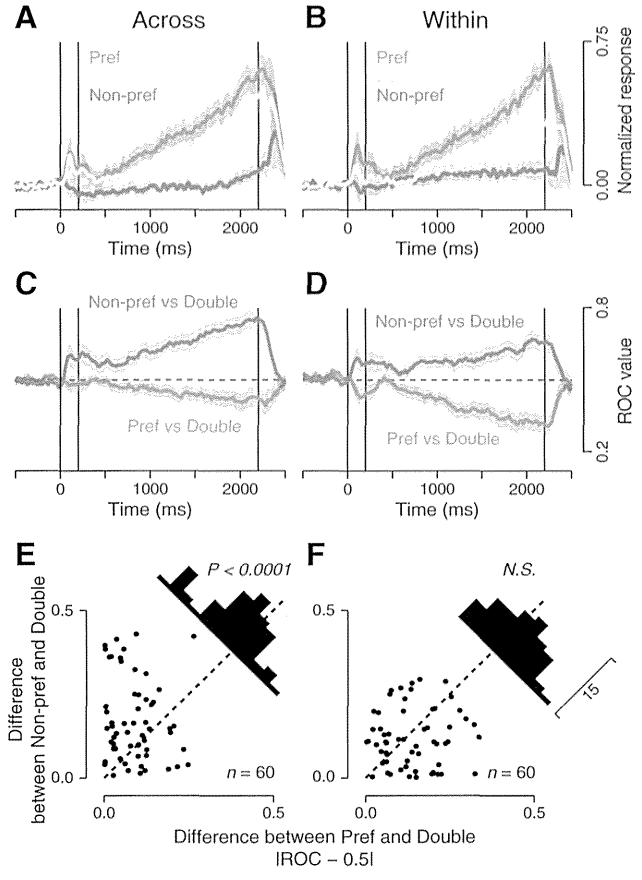

Figure 3. Comparison between the Across and Within conditions. ***A***, ***B***, Population activities in the MMS trials with two samples presented across (***A***) or within (***B***) visual field(s) (green traces) are compared with those in the SMS trials with a sample at either the preferred (red) or nonpreferred (blue) location. Shaded areas represent 95% confidence intervals. ***C***, ***D***, Population averages of the ROC values computed between the activity in the MMS and SMS trials. ROC values were taken to be 1 or 0 when activities in MMS trials were consistently higher or lower than those in any SMS trials, respectively. ***E***, ***F***, Differences in neuronal responses in the MMS and SMS trials were assessed by comparing the deviation of the ROC values from 0.5. In the Across condition (***E***), the response to the two samples was significantly closer to the response to the single sample presented at the preferred location (paired *t* test, $p < 0.0001$). In the Within condition (***F***), the response to the two samples was in between the responses to each sample presented alone ($p > 0.1$). *N.S.*, Not significant.

increments) directions, and the MMS trials with every combination of them (10 or 20 cases).

We performed an additional behavioral experiment for the analysis shown in Figure 5. Locations of test stimuli were randomly assigned to one of eight directions (0–315° with 45° increments), whereas the samples were presented at two of four oblique directions in the MMS trials (see Fig. 1*C*) or presented at one of eight directions in the interleaved SMS trials. Although the two nonmatched stimuli were not always equidistant from the matched stimulus in individual trials because of the random assignment (e.g., see Fig. 1*C*, "Across" trial), the overall angular difference did not differ between the Across and Within conditions in all monkeys (unpaired *t* test, $p > 0.6$).

Physiological procedures. Neuronal activity was recorded through tungsten electrodes (Alpha-Omega Engineering) lowered into the PFC though a 23-gauge guide tube using a micromanipulator (MO-97S; Narishige). Neuronal signals were amplified (Model 1800; A-M Systems), filtered (Model 3625; NF), and monitored online using oscilloscopes and an audio device. The waveforms of single neuronal activity were isolated using a real-time spike sorter with template-matching algorithms (MSD or ASD; Alpha-Omega Engineering). Occurrences of action potentials were time stamped and saved in files along with the eye movement and stimulus location data during the experiments (sampling rate: 1 kHz).

Histological procedures. A postmortem examination of recording sites was performed in all monkeys (see Fig. 1*D*). At the end of the experiments, the animals were deeply anesthetized with a lethal dose of sodium pentobarbital (>50 mg/kg, intraperitoneally), and several landmark pins were penetrated at known coordinates. The animals were then perfused with an 0.1 M phosphate buffer followed by 3.5% formalin. The brain was removed, blocked, and fixed with the same solution overnight. Once the brain was equilibrated with an 0.1 M phosphate buffer containing 30% sucrose, 100-μm-thick coronal sections were cut using a freezing microtome. Sections were stained with cresyl violet, and location of each task-related neuron was reconstructed according to the coordinates of electrode penetrations relative to the landmark pins.

Data analysis. Data were analyzed offline using MATLAB (MathWorks). For the population analysis (see Fig. 3), we only considered neurons with greater excitatory response to the preferred sample than those presented 90° away from it, in the SMS trials (*t* test, $p < 0.01$). Individual neuronal activities were normalized by the peak activity during a 2300 ms period starting at the sample onset and averaged to see the time course of population activities (see Fig. 3*A*,*B*). To assess linear weights for the population activities in the SMS trials with preferred ($RESP_{pref}$) or nonpreferred ($RESP_{non\text{-}pref}$) cue to explain the activity in the MMS trials ($RESP_{double}$), we computed the value ($RESP_{double} - RESP_{non\text{-}pref}$)/($RESP_{pref} - RESP_{non\text{-}pref}$). To calculate it reliably, we used the data during the last 500 ms of the delay when most neurons were highly activated. Neurons were resampled using the bootstrap procedure (1000 repetition) to estimate the 95% confidence interval (CI). For the computer simulation shown in Figure 5, we used 16 model neurons with Gaussian directional tuning ($\sigma = 30°$) centered at different directions (22.5° increment, Fig. 5*A*, gray curves).

Results

We recorded from single neurons in the macaque PFC (Fig. 1*D*). In the MMS task (Fig. 1*A*), two sample and three test stimuli were presented across a 2 s delay. Monkeys maintained a central fixation throughout the cue and delay periods and then made a saccade to a test stimulus presented at the same location as either sample (matched stimulus). Because the matched stimulus was randomly assigned to one of the two sample locations, monkeys had to remember both locations during the delay. Two samples were always presented 90° apart from each other in the MMS trials examined in the current study. As a control, we also used the SMS task (Fig. 1*B*), in which only one sample was presented. All three monkeys performed very well in the SMS (mean ± SD of the rate of correct choice: 98 ± 2%, 98 ± 3%, and 98 ± 2%, for Monkeys J, L, and O, respectively) and MMS (90 ± 7%, 94 ± 6%, and 98 ± 2%, for Monkeys J, L, and O, respectively) tasks.

Consistent with previous studies (Funahashi et al., 1989; Matsushima and Tanaka, 2012), we found neurons exhibiting a sustained response to the visual cues. A representative neuron shown in Figure 2 exhibited an elevated activity throughout the delay period after a single sample presented in the upper-left receptive field (RF, Fig. 2*A*). When the cue was located 90° away from the RF, however, the delay-period activity disappeared (Fig. 2*B*,*C*). In the MMS trials with two samples presented across the left and right visual fields (Fig. 2*D*, Across condition), the same neuron exhibited strong activity (green trace), comparable with the response to a single cue presented in the RF (red trace, same data as in Fig. 2*A*). On the other hand, when the two cues were presented within the same hemifield (Fig. 2*E*, Within condition), the neuron exhibited an intermediate response between those to the preferred (red) and nonpreferred (blue) stimulus presented alone.

Neuronal responses in the two conditions were consistently different in the sampled population. In the Across condition, the population activity for the two cues in the MMS trials (Fig. 3*A*, green trace) was similar to that for the preferred cue presented

alone (Fig. 3*A*, red trace), but far stronger than that for the nonpreferred cue (Fig. 3*A*, blue trace). On the contrary, in the Within condition, the population activity was intermediate between the activities for the individual cues (Fig. 3*B*). The linear weight of population activities was significantly biased toward the preferred cue in the Across condition (0.75, 95% CI = [0.66 0.84], bootstrap repetition = 1000), but neither cue in the Within condition (0.40, 95% CI = [0.29 0.52]). To assess the separation of responses between the MMS and SMS trials in individual neurons, we computed ROC values for every 100 ms (20 ms step). The population average shows that the ROC values for the Across condition were closer to 0.5 when responses in the MMS trials were compared with those in the SMS trials for the preferred (Fig. 3*C*, red trace), rather than the nonpreferred sample (Fig. 3*C*, blue trace), indicating that the response to the two cues was closer to the response to the single cue presented at the preferred location. On the other hand, ROC values for the Within condition were equally separated from 0.5 when compared with either sample (Fig. 3*D*), indicating that the response to the two cues differed evenly from the response to the preferred or nonpreferred cue presented alone. When we computed the mean deviation of the ROC values from 0.5 in the last 1500 ms of the delay, we found a significant difference between those for the preferred and nonpreferred samples in the Across condition (paired t test, $p < 0.001$, Fig. 3*E*), but not in the Within condition ($p > 0.1$, Fig. 3*F*). We also examined trial-by-trial response variability by computing the Fano factor during the delay but failed to find differences between the task configurations for the Across (two samples, 1.2 ± 0.5; single preferred, 1.1 ± 0.5; single nonpreferred, 1.2 ± 0.5, one-way ANOVA, $n = 60$, $p > 0.5$) and Within conditions (1.3 ± 0.5, 1.1 ± 0.5, 1.2 ± 0.4, $p > 0.4$). These results suggest that multiple locations might be represented by different firing rates of neurons depending on the relative stimulus locations. In the Across condition, neuronal activity is dominated by the preferred stimulus, almost in a winner-take-all manner. In the Within condition, neuronal activity is equally affected by individual stimuli, resulting in the average response.

Different neuronal modulations could not be attributed to other factors than the relative location across the visual fields. First, one might argue that monkeys attended to a specific sample in the Across condition. However, this is unlikely because monkeys performed equally well when the matched stimulus was presented at the preferred or nonpreferred location in the Across (preferred vs nonpreferred, 97.9 ± 4.8% vs 99.0 ± 3.1%, paired t test, $p > 0.1$) as well as in the Within condition (97.9 ± 5.8% vs 99.2 ± 2.7%, $p > 0.1$). Second, the nonpreferred stimulus might be presented inside the RF in the Within condition so that it competed with the preferred stimulus. However, as we fitted Gaussian tuning curves to delay-period activities in the SMS trials, the nonpreferred cues presented in both conditions were located 3.1 SD away from the RF center (mean ± SD, Across, 3.1 ± 1.8; Within, 3.1 ± 2.1, $n = 60$, paired t test, $p > 0.7$). Third, multiple locations might be remembered as a single entity encompassing the two samples in the Within condition. Incompatible with this, neurons tuned to the midpoint of the samples were suppressed when monkeys remembered the two locations simultaneously (Fig. 4). Furthermore, the rate of choosing the test stimuli when presented in between the two samples was much lower than the rate at the cued locations (see below, Fig. 5*C–E*). These results were analogous to those for multifocal attention; visual responses to a distractor flanked by attended objects were suppressed in the extrastriate visual area (Niebergall et al., 2011). Because the response variability was comparable between the MMS and SMS trials, the focus of working memory seemed to be divided, rather than fluctuating, between the two locations.

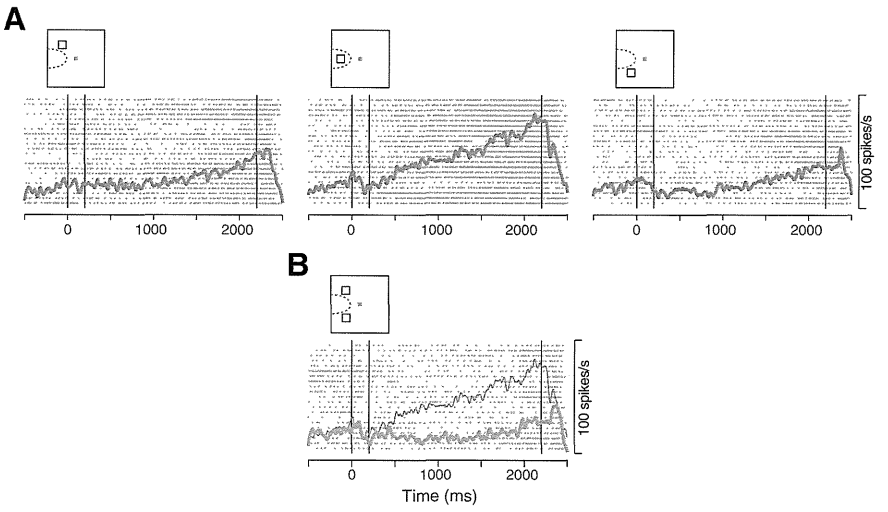

Figure 4. Activity of a neuron tuned to the midpoint of samples. ***A***, Activities in the SMS trials. This neuron exhibited a strong response to a single sample presented in the left RF (middle), but not to samples presented 45° away from the RF (left, right). ***B***, Activity in the MMS trials. The same neuron exhibited a much lower response to two samples presented within the left visual field (red thick trace) than to a single sample presented at the midpoint of them (blue thin trace; the same data as in ***A***, middle).

Based on the results of the neuronal recordings, we next attempted to simulate population activities during the delay in the MMS trials. In the Across condition where neurons responded in a "winner-take-all" manner (Fig. 5*A*, left), a neuron tuned to a specific location (black solid curve) would exhibit a comparable response to the activity for a single cue presented around its preferred location (blue dot at the level of intercept with vertical line indicating Sample 1). In the Within condition (Fig. 5*A*, right), however, the same neuron would exhibit an "Averaging" response of those to individual samples (red dot at the mean level of two intercepts). Repetition of similar computations for 16 spatially tuned neurons yielded a population coding with maximal activities at the two sample locations, both in the Across (blue) and Within conditions (Fig. 5*A*, red solid curves). This result indicates that cued locations are encoded by the most active neurons in the array, just like the previous computational model (Compte et al., 2000). However, the quality of the signal represented in the neuronal population appeared to differ between the two conditions, as further clarified by overlaying the normalized population activities (Fig. 5*B*); the activity contrast between the cued and the intermediate locations was reduced in the Within condition compared with the Across condition.

To see the corresponding behavioral outcomes, we conducted an additional experiment. In the behavioral test, one of the nonmatched stimuli was occasionally presented in between the two sample locations (Fig. 1*C*). As the choice probability was calculated for each test stimulus (Fig. 5*C–E*), we found that all monkeys made more errors in choosing the midpoint of two samples in the Within than in the Across condition (both-side z test, $p <$

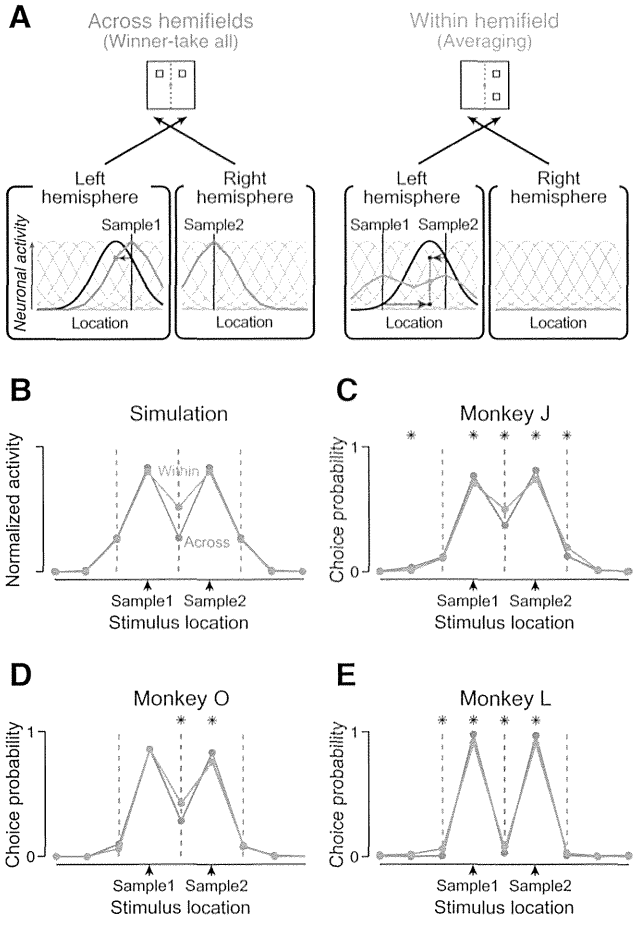

Figure 5. Model prediction and behavioral performance. ***A***, Representations of two sample locations in simulated population activities. The model assumes that the visual inputs from opposite visual fields are processed independently while those from the same visual field are processed interactively. Only contralaterally responsive neurons are shown for clarity. The neuronal modulation is large in the Across condition (blue curve) but small in the Within condition (red curve). In both conditions, the sample locations are encoded as the two peaks in the population activity. ***B***, Comparison of the population activities between the Across and Within conditions. Population activity for each condition was normalized so that the areas under the curves became equal. Blue and red vertical dashed lines indicate the vertical meridian in the Across and Within conditions, respectively. ***C–E***, Choice probability for each test stimulus was plotted as a function of its location relative to the samples, for individual monkeys. *Significant difference between the choice probabilities in the Across and Within conditions (both-side z test, $p < 0.05$). All animals made more errors in choosing the test stimulus presented at the midpoint of the samples in the Within condition.

0.05), consistent with the simulation results (Fig. 5*B*). Together, these results suggest that the interaction between neuronal representations of multiple locations might hinder the individuation of each spatial memory and ultimately could constrain behavioral performance.

Discussion

In the present study, we probed the neuronal correlates of working memory for multiple locations. When monkeys remembered two cues presented across the left and right visual fields, their neuronal activities were comparable with those for a single cue presented at the preferred location. When monkeys remembered two cues presented within the same hemifield, their neuronal activities were intermediate between the responses to individual cues. Our data might reflect an inherent, anatomical separation of contralateral and ipsilateral information processing along the visual pathways.

After the optic chiasm, visual inputs from the right visual field are transmitted to the left side of the brain, whereas those from the left visual field are transmitted to the right side. This laterality is especially evident in the early stages of cortical processing, in which RFs are confined to contralateral visual fields (Bullier, 2004). Reflecting the division into hemispheres, visual stimuli presented in opposite visual fields are more difficult to compare than those presented in the same hemifield (Banich and Belger, 1990; Sergent, 1990).

Even in the PFC, where neurons responding to contralateral and ipsilateral stimuli coexist (Rainer et al., 1998; Lennert and Martinez-Trujillo, 2013), inputs from different visual fields are known to reach distinct cortical columns (Goldman-Rakic and Schwartz, 1982). Related to this, behavioral performance is strongly influenced by the spatial arrangement of visual items even in tasks requiring higher order processing; humans can attend to (Alvarez and Cavanagh, 2005) or remember (Delvenne, 2005) more objects when presented bilaterally than unilaterally. As for the neural correlates, Buschman et al. (2011) recently showed that neuronal information about object identity is more reduced by the presence of other objects in the same compared with the opposite visual field. Our data might provide a reasonable explanation for these previous observations from the view of neuronal computation within local circuits. Signals from the same visual field are processed highly competitively and averaged through recurrent connections, whereas signals from opposite hemifields are processed almost independently and spared in distinct cortical columns.

Differences in neuronal computations were further verified by monkeys' performance. Based on the observed firing modulations, we simulated the population activities during the delay in the Across and Within conditions. The simulation can be viewed as a specific form of the normalization model proposed by Reynolds and Heeger (2009), where individual neuronal activities are normalized by the total activity in each neuronal ensemble responsible for either visual hemifield. As suggested by a previous computational model (Compte et al., 2000), we found that the cued locations could be represented by the most active neurons in the population. Thus, in our task configuration, the matched stimulus would be simply read out by detecting a peak of activity when visual responses to test stimuli were added to the population activity. However, the generally noisy activities of neurons seemed to produce an accidental peak at uncued locations, causing errors. Corresponding to the relatively higher activity at the midpoint of the two sample locations, monkeys erroneously reported the midpoint as a cued location more often in the Within than in the Across condition. These results demonstrate that the interaction of multiple representations within each neuron determines the signal-to-noise ratio in the population activity and ultimately constrains the behavioral performance. Considering the columnar organization of contralateral and ipsilateral neurons in the PFC (Goldman-Rakic and Schwartz, 1982), the interactions might be mediated by interneurons constructing recurrent network with nearby functionally related pyramidal neurons (Gabbott and Bacon, 1996; Rao et al., 1999). Because there also exist long-range horizontal connections in the cortex (Stepanyants et al., 2009), signal processing in each cortical column might not be completely independent so that the magnitude of intracolumnar and intercolumnar interactions might be relatively, rather than absolutely, different. Nonetheless, our data suggest that the relative difference is sufficient to alter the neuro-

nal signals and behavioral performance in the Across and Within conditions. Because the balanced inhibition to excitation within local circuits is essential to prevent epileptic activity (Turrigiano, 2011), the working memory capacity limited by the recurrent inhibition might be computationally (Usher and Cohen, 1999) and evolutionarily (Hultsch, 1992) inevitable.

References

Alvarez GA, Cavanagh P (2005) Independent resources for attentional tracking in the left and right visual hemifields. Psychol Sci 16:637–643. CrossRef Medline

Banich MT, Belger A (1990) Interhemispheric interaction: how do the hemispheres divide and conquer a task? Cortex 26:77–94. CrossRef Medline

Bruce CJ, Goldberg ME (1985) Primate frontal eye fields: I. Single neurons discharging before saccades. J Neurophysiol 53:603–635. Medline

Bullier J (2004) Communications between cortical areas of the visual system. In: The visual neurosciences (Chalupa LM, Werner JS, eds), pp 522–540. Cambridge, MA: Massachusetts Institute of Technology.

Buschman TJ, Siegel M, Roy JE, Miller EK (2011) Neural substrates of cognitive capacity limitations. Proc Natl Acad Sci U S A 108:11252–11255. CrossRef Medline

Compte A, Brunel N, Goldman-Rakic PS, Wang XJ (2000) Synaptic mechanisms and network dynamics underlying spatial working memory in a cortical network model. Cereb Cortex 10:910–923. CrossRef Medline

Delvenne JF (2005) The capacity of visual short-term memory within and between hemifields. Cognition 96:B79–B88. CrossRef Medline

Desimone R, Duncan J (1995) Neural mechanisms of selective visual attention. Annu Rev Neurosci 18:193–222. CrossRef Medline

Edin F, Klingberg T, Johansson P, McNab F, Tegnér J, Compte A (2009) Mechanism for top-down control of working memory capacity. Proc Natl Acad Sci U S A 106:6802–6807. CrossRef Medline

Funahashi S, Bruce CJ, Goldman-Rakic PS (1989) Mnemonic coding of visual space in the monkey's dorsolateral prefrontal cortex. J Neurophysiol 61:331–349. Medline

Fuster JM, Alexander GE (1971) Neuron activity related to short-term memory. Science 173:652–654. CrossRef Medline

Gabbott PL, Bacon SJ (1996) Local circuit neurons in the medial prefrontal cortex (areas 24a-c, 25 and 32) in the monkey: II. Quantitative areal and laminar distributions. J Comp Neurol 364:609–636. CrossRef Medline

Gnadt JW, Andersen RA (1988) Memory related motor planning activity in posterior parietal cortex of macaque. Exp Brain Res 70:216–220. Medline

Goldman-Rakic PS (1995) Cellular basis of working memory. Neuron 14:477–485. CrossRef Medline

Goldman-Rakic PS, Schwartz ML (1982) Interdigitation of contralateral and ipsilateral columnar projections to frontal association cortex in primates. Science 216:755–757. CrossRef Medline

Hikosaka O, Wurtz RH (1983) Visual and oculomotor functions of monkey substantia nigra pars reticulate: III. Memory-contingent visual and saccade responses. J Neurophysiol 49:1268–1284. Medline

Hultsch H (1992) Time window and unit capacity: dual constraints on the acquisition of serial information in songbirds. J Comp Physiol Sensory Neural Behav Physiol 170:275–280.

Kubota K, Niki H (1971) Prefrontal cortical unit activity and delayed alternation performance in monkeys. J Neurophysiol 34:337–347. Medline

Lennert T, Martinez-Trujillo JC (2013) Prefrontal neurons of opposite spatial preference display distinct target selection dynamics. J Neurosci 33:9520–9529. CrossRef Medline

Matsushima A, Tanaka M (2012) Neuronal correlates of multiple top-down signals during covert tracking of moving objects in macaque prefrontal cortex. J Cogn Neurosci 24:2043–2056. CrossRef Medline

Moran J, Desimone R (1985) Selective attention gates visual processing in the extrastriate cortex. Science 229:782–784. CrossRef Medline

Niebergall R, Khayat PS, Treue S, Martinez-Trujillo JC (2011) Multifocal attention filters targets from distracters within and beyond primate MT neurons' receptive field boundaries. Neuron 72:1067–1079. CrossRef Medline

Rainer G, Asaad WF, Miller EK (1998) Memory fields of neurons in the primate prefrontal cortex. Proc Natl Acad Sci U S A 95:15008–15013. CrossRef Medline

Rao SG, Williams GV, Goldman-Rakic PS (1999) Isodirectional tuning of adjacent interneurons and pyramidal cells during working memory: evidence for microcolumnar organization in PFC. J Neurophysiol 81:1903–1916. Medline

Reynolds JH, Heeger DJ (2009) The normalization model of attention. Neuron 61:168–185. CrossRef Medline

Rigotti M, Barak O, Warden MR, Wang XJ, Daw ND, Miller EK, Fusi S (2013) The importance of mixed selectivity in complex cognitive tasks. Nature 497:585–590. CrossRef Medline

Sergent J (1990) Furtive incursions into bicameral minds: integrative and coordinating role of subcortical structures. Brain 113:537–568. CrossRef Medline

Stepanyants A, Martinez LM, Ferecskó AS, Kisvárday ZF (2009) The fractions of short- and long-range connections in the visual cortex. Proc Natl Acad Sci U S A 106:3555–3560. CrossRef Medline

Tanaka M (2005) Involvement of the central thalamus in the control of smooth pursuit eye movements. J Neurosci 25:5866–5876. CrossRef Medline

Treue S, Maunsell JH (1996) Attentional modulation of visual motion processing in cortical areas MT and MST. Nature 382:539–541. CrossRef Medline

Turrigiano G (2011) Too many cooks? Intrinsic and synaptic homeostatic mechanisms in cortical circuit refinement. Annu Rev Neurosci 34:89–103. CrossRef Medline

Usher M, Cohen JD (1999) Short term memory and selection processes in a frontal-lobe model. In: Connectionist models in cognitive neuroscience, pp 78–91. London: Springer.

Warden MR, Miller EK (2007) The representation of multiple objects in prefrontal neuronal delay activity. Cereb Cortex 17[Suppl 1]:i41–i50.

Wei Z, Wang XJ, Wang DH (2012) From distributed resources to limited slots in multiple-item working memory: a spiking network model with normalization. J Neurosci 32:11228–11240. CrossRef Medline

Systems/Circuits

Differential Neuronal Representation of Spatial Attention Dependent on Relative Target Locations during Multiple Object Tracking

Ayano Matsushima and Masaki Tanaka
Department of Physiology, Hokkaido University School of Medicine, Sapporo 060-8638, Japan

Humans can simultaneously track multiple moving objects with attention. The number of objects that can be tracked is known to be larger when visual stimuli are presented bilaterally rather than presented unilaterally. To elucidate the underlying neuronal mechanism, we trained monkeys to covertly track a single or multiple object(s). We found that neurons in the lateral prefrontal cortex exhibited greater activity for the target passing through the receptive field (RF) than for distractors. During multiple-object tracking, response enhancement for one target presented in the RF was stronger when the other target was located in the opposite than the same visual hemifield. Because the neuronal modulation did not differ depending on relative target locations with respect to upper and lower visual hemifields, the distance between the targets does not explain the results. We propose that inherent, anatomical separation of visual processing for contralateral and ipsilateral visual fields might constrain cognitive capacity.

Key words: attentional capacity; bilateral advantage; MOT; prefrontal cortex; primate; single-unit recording

Introduction

Along the visual processing pathways, the left visual field is represented in the right hemisphere and the right visual field is represented in the left hemisphere. This laterality is especially evident in the early stages of visual processing, but is relaxed for higher order processing in the association cortices where information from both visual hemifields are integrated (Desimone et al., 1993; Rainer et al., 1998). This integration process must be mediated via the commissural connections, which unify the representation of the entire visual field.

Deviation from the above principle may occur in split-brain patients (Gazzaniga, 1970). Although disconnected cerebral cortices can exchange crude visual information, they cannot communicate details about features, locations (Holtzman, 1984), or time (Corballis et al., 1998). Conversely, split-brain patients are less annoyed by interference across the midline when stimuli are presented bilaterally, exhibiting superior performances to normal subjects in the Stroop task (David, 1992), dual task paradigm (Holtzman and Gazzaniga, 1985), and visual search (Luck et al., 1989). Thus, the compromised interhemispheric integration can hinder or benefit the performance depending on whether the task requires integration or separation of information from different visual hemifields.

Even in normal subjects, the integration across hemifields has been shown to be incomplete. In the tasks requiring direct comparison of multiple objects (Banich and Belger, 1990; Sergent, 1990) or integration of visual information across time (Dimond et al., 1972), performance is impaired when the stimuli are divided into the left and right visual fields. However, in the tasks requiring parallel processing of individual objects, performance is improved when the stimuli are presented across hemifields compared with within a hemifield (Sereno and Kosslyn, 1991; Awh and Pashler, 2000; Scalf et al., 2007). These costs and benefits of bilateral display are most evident when the task is rather demanding (Merola and Liederman, 1990; Kraft et al., 2005) and requires spatial information processing (Delvenne, 2005).

At the neuronal level, evidence has recently accumulated for parallel processing of two visual hemifields. When two visual stimuli were presented bilaterally, prefrontal activities were initially dominated by the contralateral stimulus, and thereafter evolved to represent the task-relevant object (Kadohisa et al., 2013). In addition, when monkeys remembered the locations (Matsushima and Tanaka, 2014b) or identities (Buschman et al., 2011) of multiple objects, neuronal information for a given object was not, if any, degraded when all other objects were in the opposite hemifield. These results suggest that neuronal processing for visual discrimination and working memory is more efficient for bilateral than unilateral stimuli. However, it remains elusive whether the attentional allocation toward the targets also depends on their relative locations across the hemifields, while keeping it away from the other, task-irrelevant stimuli.

To address this issue, we examined neuronal activities of prefrontal neurons during monkeys attentively tracked two targets

Received March 22, 2014; revised May 6, 2014; accepted June 13, 2014.

Author contributions: A.M. and M.T. designed research; A.M. performed research; A.M. contributed unpublished reagents/analytic tools; A.M. analyzed data; A.M. and M.T. wrote the paper.

This work was supported by grants from the Ministry of Education, Culture, Sports, Science and Technology of Japan, the Ministry of Health, Labour and Welfare of Japan, the Japan Society for the Promotion of Science, the Takeda Science Foundation, and the Smoking Research Foundation. Animals were provided by the National Bio-Resource Project. We thank T. Mori and A. Hironaka for the animal care, M. Suzuki for administrative help, and all lab members for comments and discussions.

The authors declare no competing financial interests.

Correspondence should be addressed to Dr Ayano Matsushima, Department of Neurochemistry, Graduate School of Medicine, The University of Tokyo, 7-3-1 Hongo, Bunkyo-ku, Tokyo, Japan. E-mail: ayano@m.u-tokyo.ac.jp.

DOI:10.1523/JNEUROSCI.4354-13.2014

 0270-6474/14/349963-07$15.00/0

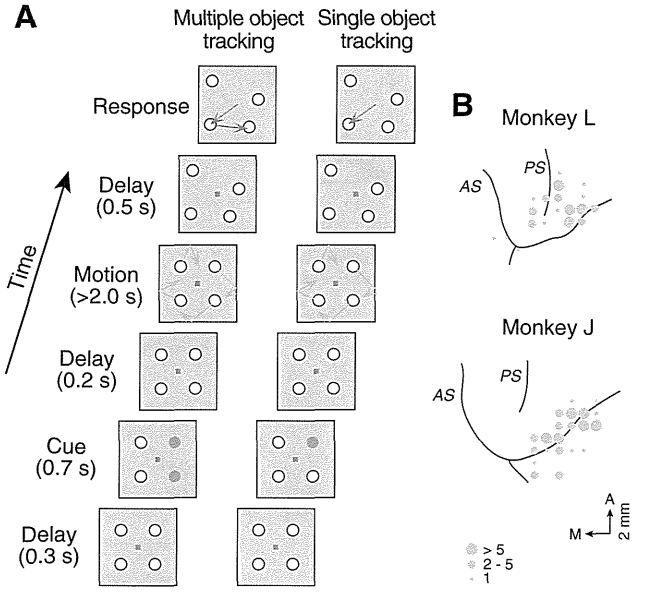

Figure 1. Behavioral paradigms. ***A***, In the MOT task (left), four visual stimuli were presented during central fixation. Two objects were cued as targets, whereas the others served as distractors. Following a short delay, all objects moved randomly for >2 s. In response to the FP offset, monkeys made sequential saccades to the targets. Because the objects were visually identical except during the cue period, monkeys needed to covertly track the target motions. In the SOT task (right), only one object was cued as a target. ***B***, Recording sites. The size of each circle indicates the number of neurons recorded from each penetration. PS, Principal sulcus; AS, arcuate sulcus.

in the presence of distractors. We found stronger response to the targets presented bilaterally than those presented unilaterally, which might explain the different tracking capacity of humans under the two conditions (Alvarez and Cavanagh, 2005; Hudson et al., 2012).

Materials and Methods

Experiments were conducted on two Japanese macaques (*Macaca fuscata*, 6–7 kg females). All animal protocols were approved by the Animal Care and Use Committee of Hokkaido University. The procedure of animal preparation is described previously in detail (Tanaka, 2005). Briefly, a pair of head holders was implanted on the skull and a coil of stainless steel wire was implanted under the conjunctiva under isoflurane anesthesia. During training and experimental sessions, the monkey's head was secured to the primate chair, and eye position was recorded using the search coil technique (MEL-25; Enzanshi Kogyo). After training, a recording cylinder was installed over a small craniotomy. Animals received analgesia after each surgery. The monkeys' water intake was controlled daily to motivate them to perform the tasks.

Visual stimuli and behavioral paradigms. Experiments were controlled by a Windows-based real-time data acquisition system (TEMPO; Reflective Computing). Visual stimuli were presented on a 24 inch CRT monitor (GDM-FW900, refresh rate 60 Hz; Sony) positioned 38 cm from the eyes (subtending 64° × 44° of visual angle), located in a darkened booth. All visual stimuli were presented within a 36° square contour that was visible throughout the experiments. Each trial began with the appearance of a fixation point (FP; 0.5° red square) at the screen center, and ended with a juice reward for correct performance.

In the multiple-object tracking (MOT) task (Fig. 1*A*, left), four visual stimuli (1.5° white circles) were presented at 10° eccentricity during central fixation. Their initial locations and motion directions were defined in polar coordinates, and angles were chosen randomly from 0° to 350° (10° increments, measured from rightward) for each object. The separation of polar angles between any two stimuli was set to be ≥50°, for both the initial locations and motion directions. Two objects were cued as targets by briefly changing their color (red, 700 ms), whereas the other objects remained white and served as distractors. Except for this cue period, all objects were identical in color and shape. Following a 200 ms delay, four objects moved along straight paths at 20°/s in different directions without visible trails and bounced against the sides of the contour (motion period: 2500 ms for Monkey J, 2000 ms for Monkey L). Each object could move into the other quadrants than the initial location. Monkeys were required to keep their eyes within 5° of the FP throughout the motion and following delay (500 ms) periods, and make two sequential saccades to the targets. To obtain reward, the animals needed to make the initial saccade within 400 ms of the FP offset and to redirect their eyes to the other target in 400 ms thereafter. When any object was located within 7° from the FP or the distance between any two objects was <6°, the motion interval was extended until neither condition was fulfilled. We also introduced the single-object tracking (SOT) task (Fig. 1*A*, right) as a control. This task was identical to the MOT task except that only one object was cued as a target.

Once the animals performed correctly in a MOT trial, the object trajectories in the subsequent seven MOT trials and eight SOT trials were automatically determined to balance the object trajectories across trials (Fig. 2*A*, bottom). In three MOT trials, the object trajectories were identical to the initial successful trial but the assignment of object identities was rotated one by one. In the other four MOT trials, the object trajectories were point symmetry of those in the above-described MOT trials with respect to the central FP. In the eight SOT trials, the object trajectories were exactly the same as the MOT trials. Thus, once monkeys performed a MOT trial correctly, the object trajectories in the following 15 trials were determined automatically, and were presented in a pseudorandom order.

Physiological procedures. Neuronal activity was recorded through tungsten electrodes (Alpha Omega Engineering) lowered into the prefrontal cortex (PFC) through a 23 gauge guide tube using a micromanipulator (MO-97S; Narishige). Signals were amplified (Model 1800; A-M Systems), filtered, and monitored online using oscilloscopes and an audio device. Waveforms of single neurons were isolated using a real-time spike sorter with template-matching algorithms (MSD or ASD; Alpha Omega Engineering). Occurrences of action potentials were time stamped and saved in files with the data for eye movements and stimulus locations (sampling rate, 1 kHz).

Verification of recording sites. A postmortem examination of recording sites was performed in all monkeys (Fig. 1*B*). At the end of the experiments, the animals were deeply anesthetized with a lethal dose of sodium pentobarbital (> 50 mg/kg, intraperitoneally), and several landmark pins were penetrated at known coordinates. The animals were then perfused with 0.1 M phosphate buffer followed by 3.5% formalin. The brain was removed, blocked, and fixed with the same solution overnight. Location of each task-related neuron was reconstructed according to the coordinates of electrode penetrations relative to the landmark pins.

Data analysis. Data were analyzed offline using MATLAB (MathWorks). We considered only neurons that were tested for >80 trials ($n = 137$). To assess the firing modulation depending on the target and distractor locations during the motion period, the instantaneous firing rate was calculated as a function of each object location on the retina (i.e., location on the screen minus eye position in the orbit). Initially, each object location 60 ms before the occurrence of action potentials was plotted separately, with a 0.5° resolution. Then, the number of action potentials was divided by the duration of each object presentation to obtain the firing rate for each pixel (0.5° square). Data were filtered using a 2-D Gaussian kernel ($\sigma = 2.5°$, 20° square), and presented as a color-coded map ("response modulation map").

For individual neurons, we defined the RF in the response modulation map for target locations in the SOT trials as the region with 477 adjacent pixels (10% of whole map) that gave the maximal mean firing rate. The RF center was defined as the center of gravity weighted by the firing rate for each of the 477 pixels. In Figure 3, we examined whether the response to one target in the RF was modulated depending on whether the other target appeared in the different ("Across" condition) or same ("Within" condition) visual hemifield. To reliably distinguish these conditions, we only considered neurons with RF centers that were ≥6° eccentricity and located ≥3° away from the cardinal meridians (83/137, 61%).

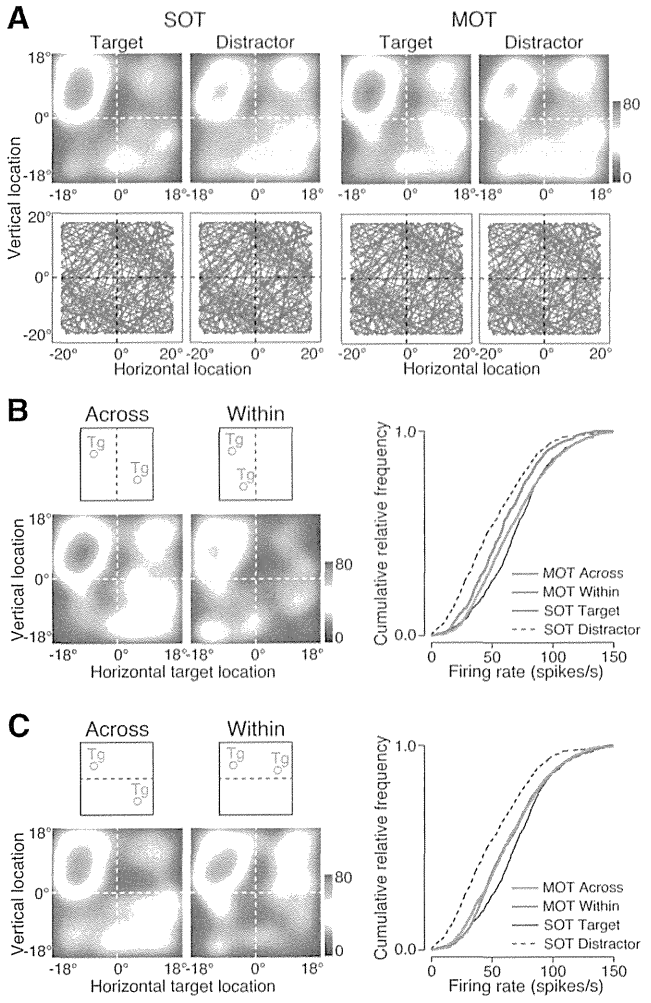

Figure 2. Activity of a representative prefrontal neuron. ***A***, Activity of a single neuron in the SOT and MOT trials. Instantaneous firing rates during the motion periods are color-coded as a function of each object locations (top). Note that the target and distractor trajectories were exactly the same across the trials, because they were interchanged from trial to trial (bottom; see Materials and Methods). ***B***, Data for the MOT trials were divided into two groups according to relative target locations. Right, Plot of the cumulative distributions of millisecond-by-millisecond firing rates for the targets presented in the upper-left RF under the Across (red) and Within (blue) conditions. Black solid and dotted lines indicate the data for the target and distractors, respectively, presented in the RF during the SOT trials. Medians differed significantly between the Across and Within conditions (Wilcoxon rank sum test, $p < 0.0001$), whereas the variances did not (Ansari-Bradley test, $p > 0.05$). ***C***, When the same data were divided according to relative target locations in the upper/lower visual hemifields, the activities were not different (median, $p = 0.54$; variance, $p = 0.29$).

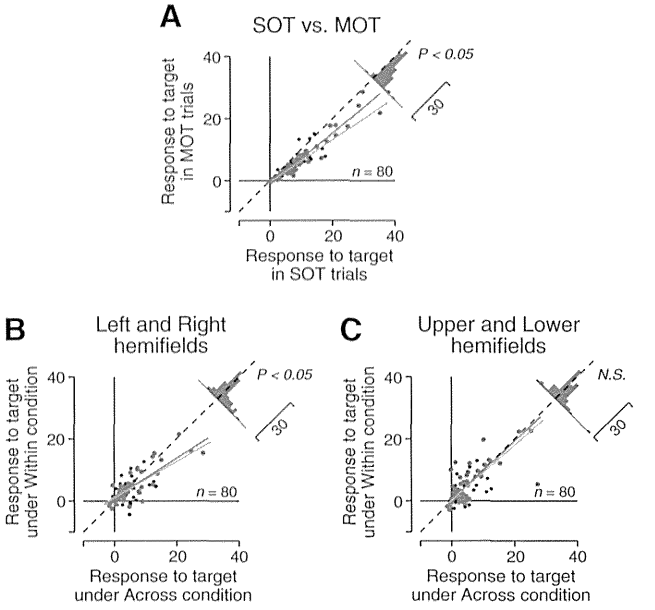

Figure 3. Population analyses for neuronal modulation by relative target locations. ***A***, Response to the target was compared between the SOT and MOT trials for individual neurons. In the population, the firing rate decreased in the MOT trials (paired t test, $p < 0.05$). ***B***, ***C***, Comparison of the response in the MOT trials under different conditions. With respect to the right/left visual hemifields (***B***), the activity was significantly greater under the Across than the Within condition (paired t test, $p < 0.05$). However, there was no difference with respect to the upper/lower visual hemifields (***C***; $p = 0.45$). Red lines indicate robust linear regressions (***A***–***C***). Blue dots and lines indicate the data for 48 neurons that showed a significant difference between conditions even when the data with equal intertarget distance were considered (see Results).

To estimate the null response modulations observed by chance, we shuffled the correspondence between spike data and object trajectories in individual neurons, and computed a "sham" response modulation map (Matsushima and Tanaka, 2012). We repeated this shuffling procedure 1000 times to obtain the distribution of variance of firing rates across the field, expected by chance. Neurons exhibiting a significant firing modulation for the target in the SOT trials ($p < 0.05$, 82/83, 99%) were included for further analyses.

For the population analysis shown in Figures 3 and 4, the response to the targets in the RF was calculated by subtracting the mean firing rates in the whole response modulation map. To directly rule out the possibility that the Across versus Within difference stems from the different target separations, we compared neuronal responses to the two targets separated by a same distance but located within or across the visual fields. In search of the optimal target separation, we first plotted the firing rates as a function of target separations (bin width = 10°, 1° increments), regardless of the Across/Within conditions. To disregard data when both targets were within the RF, bins centered ≤1.5 times of the maximum point separation within the RF were excluded from the analysis. If the optimal target separation lasted for >1000 ms in total, for both the Across and Within conditions, we compared the distributions of millisecond-by-millisecond firing rates (filtered by Gaussian with 30 ms σ) between the conditions. In a few neurons (4/80, 5%), above criteria left no bins to be analyzed.

Results

We recorded from single neurons in the PFC close to the frontal eye fields while monkeys covertly tracked moving object(s) without eye movements (Fig. 1*A*). During recording sessions, both monkeys performed very well. Deviation of eye position from the center of the FP during covert tracking averaged 0.68° ± 0.11° (SD) and 0.73° ± 0.10° for Monkeys J and L, respectively. Both monkeys correctly chose targets in the SOT (mean ± SD, 77.5 ± 7.6% and 88.2 ± 6.0% for Monkeys J and L, respectively) and the MOT trials (64.7 ± 10.0% and 54.4 ± 7.2%), well above the chance level (25% for SOT or 8.3% for MOT trials).

Regardless of the number of objects to be tracked, PFC neurons consistently signaled the target positions during the motion period. Figure 2*A* shows the response modulation maps for a representative neuron. In the SOT trials (Fig. 2*A*, two top left panels), this neuron exhibited enhanced activity as the target passed through the upper-left RF, whereas the activity was less for the distractor presented at the same location. Since the trajectories of the target and distractor were exactly balanced across the trials (Fig. 2A, two bottom left panels), the difference in response must be attributed to their different meanings in the task. Although neuronal response to the stimulus outside of the RF ap-

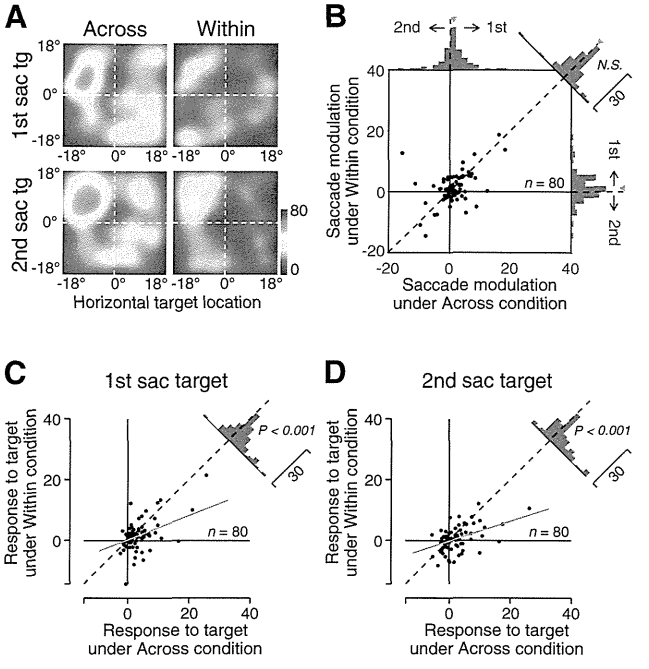

Figure 4. Lack of correlation between neuronal modulations by relative target location and saccade order. ***A***, Data of the neuron shown in Figure 2 were divided into four groups according to whether the two targets were located unilaterally or bilaterally during motion periods and whether the target was selected by the first or second saccade after the motion end. ***B***, Comparison of neuronal modulation depending on saccade order in the Across and Within conditions. Saccade modulation was defined as the difference of response to the targets for the first and second saccades ($RESP_{first} - RESP_{second}$). Red arrowheads indicate the averages across the population. ***C***, Response to the first saccade target presented in the RF was compared between conditions where the other target was located in the opposite (Across) or same (Within) visual hemifield. ***D***, Comparison of response to the second saccade target between the Across and Within conditions. Red lines indicate robust linear regressions (slopes are 0.40 and 0.33 in ***C*** and ***D***, respectively).

peared to be somewhat larger for the distractor than for the target, it was merely a consequence of the enhanced response to the target presented in the RF, because the same spike data were sorted by the target and distractor locations, respectively. The pattern of neuronal modulation was consistent with our previous results of the Target-selective prefrontal neurons in a similar SOT task (Matsushima and Tanaka, 2012), and those reported in the extrastriate visual areas (Mitchell et al., 2007; Niebergall et al., 2011a). In the MOT trials, the same neuron again exhibited a greater response to the target than to the distractor presented in the RF (Fig. 2*A*, two top right panels), indicating that this neuron was involved in the representation of multiple as well as single-target locations.

We next examined whether the response to the target in the RF depended on the relative locations of two targets in the MOT trials. We divided the data into two groups, according to whether the targets were presented bilaterally or unilaterally. When the two targets were located across the left and right visual hemifields (Across condition), the neuronal response to the target was strong (Fig. 2*B*, left). However, when the two targets were located within either visual hemifield (Within condition), the response was reduced (Fig. 2*B*, middle). To quantitatively compare these two conditions, we computed the millisecond-by-millisecond firing rates (filtered by Gaussian with 30 ms σ) while the target was presented in the RF, and found that the response was statistically greater under the Across than Within conditions (Wilcoxon rank sum test, $p < 0.0001$; Fig. 2*B*, right). As a control analysis, we also divided the same data according to whether the targets were presented across or within the upper/lower visual hemifields, and found no difference between the conditions ($p = 0.54$; Fig. 2*C*).

Selective enhancement of response to the target, and the reduced target response in the Within condition were also observed across the population we studied. Among 82 neurons exhibiting significant firing modulation in the SOT trials (Methods), 80 (98%) neurons also showed a significant modulation in the MOT trials. However, the magnitude of the response to the target was slightly but significantly less in the MOT than in the SOT trials (paired t test, $p < 0.05$; Fig. 3*A*), with a robust regression slope of 0.68, (significantly different from 1, t test, $p < 0.0001$). As the data were sorted according to the relative target locations, the response was greater when the two targets were presented across the left and right visual hemifields (Across condition) than when presented within either hemifield (Within condition, $p < 0.05$; Fig. 3*B*). Accordingly, the robust regression analysis yielded the slope of 0.58 that significantly differed from the unity line ($p < 0.0001$). In contrast, there was no significant difference between the Across and Within conditions with regard to the upper versus lower visual hemifields ($p = 0.45$; Fig. 3*C*), and the robust regression slope did not differ from 1 (0.89, $p > 0.1$). The significant difference in the whole population indicates that the target representation in the PFC was degraded when both targets were presented unilaterally, which might cause an overall reduction of firing modulation in the MOT trials compared with the SOT trials (Fig. 3*A*).

Different neuronal modulation for targets presented within and across hemifields during motion periods were unlikely to be related to the difference in saccade directions, because targets moved randomly before the execution of saccades. Nevertheless, because we previously showed that prefrontal activities biased the selection of an object to be tracked then targeted by a saccade at the trial end (Matsushima and Tanaka, 2014a), neuronal activities during the motion periods might control the saccade orders at the end of the MOT trials. To see whether saccade orders could account for the differential response between the Across and Within conditions, we further divided the data according to the saccade order. Although some neurons exhibited a slight difference (Fig. 4*A*; top versus bottom, for the neuron shown in Fig. 2), the magnitude of neuronal modulation by saccade orders was comparable between the Across and Within conditions in the population (paired t test, $p > 0.9$; Fig. 4*B*). Furthermore, the response to the target presented in the RF was consistently larger in the Across than Within condition, regardless of whether the target was selected by the first (Fig. 4*C*) or second (Fig. 4*D*) saccade. Thus, the difference in neuronal activity between the conditions could not be attributed to the serial order of targeting saccades. Although the neuronal control of saccade sequence is an interesting issue to be addressed (Histed and Miller, 2006), it appears to be far beyond the scope of this study.

One might argue that the difference between the Across and Within conditions could be merely a consequence of surround suppression geometry. However, surround suppression from distractors was unlikely to explain the results. We searched for the Across condition where a target was presented in the RF and both distractors were presented either in the same or opposite hemifield. For 13 neurons that fulfilled these criteria, neuronal activities remained unchanged regardless of the distractor locations (paired t test, $p = 0.15$). Furthermore, the Across/Within difference could not be attributed to the relative distance between the targets. When the millisecond-by-millisecond firing rates of in-

dividual neurons were compared when the targets were presented within or across visual fields but separated by a same distance (see Materials and Methods), the majority of neurons (48/76, 63%) exhibited higher activity in the Across than Within conditions (t test, $p < 0.05$). We further confirmed that the restriction of the analysis shown in Figure 3 to these 48 neurons reproduced the main results (Fig. 3, blue dots); the robust regression slope significantly differ from 1 for the comparison between the Across and Within conditions with regard to the left/right visual hemifields (0.64; Fig. 3*B*, blue line; t test, $p < 0.0001$), but was not with regard to the upper/lower visual hemifields (0.95; Fig. 3*C*, blue line; t test, $p > 0.1$). Thus, prefrontal neurons exhibited greater response when the two targets were presented bilaterally than unilaterally, and that these modulations could not be accounted for other factors than the relative target locations across the left and right visual fields.

As an additional analysis, we examined the variability of neuronal activity to assess whether the response reliability was also altered. For example, for the neuron shown in Figure 2, the variance of response to the target in the RF was larger in the MOT than in the SOT trials (Ansari-Bradley test, $p < 0.05$). However, the effect of the task condition was not consistent across the population; the variance of neuronal activity in the MOT trials could be larger than (16%, 13/80), smaller than (41%, 33/80), or comparable with (43%, 34/80) that in the SOT trials. Similarly, the effect of relative target locations on the response variance was not evident for the majority of neurons (41/80, 53%, $p > 0.05$) including the one in Figure 2*B*, whereas the activity of the remaining neurons was either less (22/80, 27%) or more (16/80, 20%) variable in the Across than Within conditions. To assess the overall trend, we computed Fano factors by normalizing the variance of firing rates by their mean for individual neurons. For both comparisons between the tasks (i.e., MOT vs SOT) and between the Across/Within conditions, Fano factors were not significantly different ($n = 80$, paired t test, $p > 0.1$), indicating that the response reliability remained unchanged in the population as a whole.

Discussion

We examined single neuron activities in the PFC while monkeys covertly tracked a single or multiple moving target(s) among visually identical distractors. We found that the same set of neurons elevated the activity for the target presented in the RF, regardless of the number of objects to be tracked. Enhancement of the response to a target was greater when the other target was located in the opposite than the same visual hemifield. Because the neuronal activity did not alter depending on the relative target locations with respect to the upper/lower rather than the right/left visual fields, the distance between the targets should not account for the results. Considering the inherent, anatomical separation of contralateral and ipsilateral visual processing, our data might reflect the stronger interaction of attentional signals for multiple targets presented unilaterally than those presented bilaterally.

Interaction of information processing within and across visual hemifields

During multiple-object tracking, prefrontal neurons exhibited greater activity for the target in the RF when the other target was presented in the opposite than the same visual field. Different neuronal modulation between the Across and Within conditions were likely to reflect different amount of interaction in neuronal networks; signals from opposite visual fields are processed separately, whereas those from the same visual field are interacted and processed together within the same functional module.

What network configurations are responsible for such a functional module of visual processing? One possible structure is the cerebral hemisphere. Anatomically, after the optic chiasm, visual inputs from the left and right visual fields are divided into different optic tracts. The separation is precisely retained in the early visual cortices, where neurons in each hemisphere are exclusively responsive to contralateral stimuli (Bullier, 2004). Although commissural connections somewhat alleviates the hemispheric independence in higher-order cortical areas (Myers and Sperry, 1958), much stronger association fibers within the hemispheres results in the contralateral dominance of visual processing in the inferotemporal (Chelazzi et al., 1998) and prefrontal (Funahashi et al., 1989; Lennert and Martinez-Trujillo, 2013) cortices. Indeed, inactivation of the PFC has demonstrated the contralateral bias of mnemonic (Funahashi et al., 1993) or attentional (Heide and Kömpf, 1998) deficits, indicating that the functional division between hemispheres is, on the whole, preserved in the PFC. In addition, other anatomical structures, such as the cortical columns, might further dissociate visual processing in the opposite visual fields. In the PFC, commissural fibers from the contralateral counterpart are known to terminate in columns that are distinct from, and interdigitated with, those receiving association fibers from the ipsilateral parietal cortex (Goldman-Rakic and Schwartz, 1982). Consistent with this, most prefrontal interneurons have similar response properties to nearby pyramidal neurons (Rao et al., 1999), indicating that they form locally confined functional columns with balanced excitation and inhibition (Marino et al., 2005). All of these results suggest that, from early to late stages of visual processing, signals from opposite visual fields are processed relatively independently in different functional modules, compared with those from the same visual field that undergo highly competitive interaction through lateral inhibitions. Thus, the different neuronal modulation for targets presented within and across hemifields observed here is likely to inherit the division of contralateral and ipsilateral information in the upstream structures and be maintained though the local circuit organizations within the PFC.

Among many brain regions along the visual processing pathways, the PFC is most likely to limit the tracking capacity in the MOT task. We have previously demonstrated that prefrontal neurons consistently discriminate the visually identical objects during covert tracking, that the attenuation of the signals results in erroneous choice (Matsushima and Tanaka, 2012), and that the perturbation of the signals can alter the target selection (Matsushima and Tanaka, 2014a). It is also consistent with the widely accepted view that the PFC is crucial for performing tasks with high cognitive demands (Kane and Engle, 2002; Marois and Ivanoff, 2005), especially such as precise object recognition and discrimination (Duncan et al., 1995; Buschman and Miller, 2007), and with the fact that the bilateral advantage is observed only when irrelevant objects are presented along with the targets (Holt and Delvenne, 2014).

One might argue that the difference in neuronal response to the bilateral versus unilateral targets reported in this study was modest relative to that reported previously (Kadohisa et al., 2013). Although the large difference in experimental conditions might be the major cause, there might be several other possible reasons. First, the hemispheric independence might be largest in the PFC during the initial competition between the visual stimuli. Kadohisa et al. (2013) found that, when the target and distractor were presented alone in each hemifield, prefrontal activity was

initially biased toward the contralateral stimulus regardless of its identity and then evolved to predominantly encode the target regardless of its location. During the motion periods, however, monkeys had already identified and directed attention to the targets, while ignoring the other, task-irrelevant distractors. Second, the interference on the target processing from another target, addressed in the present study, might be stronger than that from the distractor examined previously (Kadohisa et al., 2013). Because distractors are known to impede the target processing further as they serve as a target in a training history (Bichot et al., 1996; Ipata et al., 2006; Kadohisa et al., 2013), the processing conflict might be maximized between the two, equally task-relevant targets to corrupt the independence of each hemifield. Taking all these factors into consideration, the present data appeared to be compatible with the previous observations, although our data provided a first evidence that the attentional enhancement of response to multiple targets depended on relative target locations, even after the priority over the distractors was fully established.

Parallel versus serial control of attention for multiple objects

Since Pylyshyn and Storm (1988) first devised the MOT task, several models of neuronal processing have been proposed. Although each model has unique properties, one of the major differences resides in whether attention is allocated to individual targets (Pylyshyn, 1989; Kahneman et al., 1992) or to a group of targets (Yantis, 1992). In support of the latter hypothesis, subjects sometimes have introspections that the multiple targets constitute a virtual polygon (Alvarez and Cavanagh, 2005). In the current study, however, we found that the same population of neurons exhibited enhanced activity and represented target locations in both the MOT and SOT trials, suggesting that attention might be separately directed toward each of the multiple targets. These results might be attributed to the lack of similarity or symmetry of target motions in our experimental conditions, under which perceptual grouping would be difficult (Koffka, 1935).

How is attention allocated to multiple objects? There is a long-standing debate between two hypotheses (Townsend, 1990). Attention might be focused on one location at a given moment and shifted sequentially (Treisman and Gelade, 1980; Wolfe, 1994), or alternatively, divided into multiple foci simultaneously for parallel processing (Duncan and Humphreys, 1989; Godijn and Theeuwes, 2003; Niebergall et al., 2011b). Although the comparable response variability between the MOT and SOT trials in the sampled neuronal population favored the latter hypothesis, the inconsistency across individual neurons prevented us from drawing any firm conclusion. Low firing rates of PFC neurons further complicated the analysis of oscillatory transition on the scale of a few tens or hundreds of milliseconds (Horowitz et al., 2009; Chakravarthi and VanRullen, 2011). Future studies would need more intricate investigations to address this issue.

References

Alvarez GA, Cavanagh P (2005) Independent resources for attentional tracking in the left and right visual hemifields. Psychol Sci 16:637–643. CrossRef Medline

Awh E, Pashler H (2000) Evidence for split attentional foci. J Exp Psychol Hum Percept Perform 26:834–846. CrossRef Medline

Banich MT, Belger A (1990) Interhemispheric interaction: how do the hemispheres divide and conquer a task? Cortex 26:77–94. CrossRef Medline

Bichot NP, Schall JD, Thompson KG (1996) Visual feature selectivity in frontal eye fields induced by experience in mature macaques. Nature 381:697–699. CrossRef Medline

Bullier J (2004) Communications between cortical areas of the visual system. In: The visual neurosciences (Chalupa LM, Werner JS, eds), pp 522–540. Cambridge, MA: MIT.

Buschman TJ, Miller EK (2007) Top-down versus bottom-up control of attention in the prefrontal and posterior parietal cortices. Science 315:1860–1862. CrossRef Medline

Buschman TJ, Siegel M, Roy JE, Miller EK (2011) Neural substrates of cognitive capacity limitations. Proc Natl Acad Sci U S A 108:11252–11255. CrossRef Medline

Chakravarthi R, VanRullen R (2011) Bullet trains and steam engines: exogenous attention zips but endogenous attention chugs along. J Vis. 11(4):12 1–12. CrossRef Medline

Chelazzi L, Duncan J, Miller EK, Desimone R (1998) Responses of neurons in inferior temporal cortex during memory-guided visual search. J Neurophysiol 80:2918–2940. Medline

Corballis MC, Boyd L, Schulze A, Rutherford BJ (1998) Role of the commissures in interhemispheric temporal judgments. Neuropsychology 12:519–525. CrossRef Medline

David AS (1992) Stroop effects within and between the cerebral hemispheres: studies in normals and acallosals. Neuropsychologia 30:161–175. CrossRef Medline

Delvenne JF (2005) The capacity of visual short-term memory within and between hemifields. Cognition 96:B79–B88. CrossRef Medline

Desimone R, Moran J, Schein SJ, Mishkin M (1993) A role for the corpus callosum in visual area V4 of the macaque. Vis Neurosci 10:159–171. CrossRef Medline

Dimond SJ, Gibson AR, Gazzaniga MS (1972) Cross field and within field integration of visual information. Neuropsychologia 10:379–381. CrossRef Medline

Duncan J, Humphreys GW (1989) Visual search and stimulus similarity. Psychol Rev 96:433–458. CrossRef Medline

Duncan J, Burgess P, Emslie H (1995) Fluid intelligence after frontal lobe lesions. Neuropsychologia 33:261–268. CrossRef Medline

Funahashi S, Bruce CJ, Goldman-Rakic PS (1989) Mnemonic coding of visual space in the monkey's dorsolateral prefrontal cortex. J Neurophysiol 61:331–349. Medline

Funahashi S, Bruce CJ, Goldman-Rakic PS (1993) Dorsolateral prefrontal lesions and oculomotor delayed-response performance: evidence for mnemonic "scotomas." J Neurosci 13:1479–1497. Medline

Gazzaniga MS (1970) The bisected brain. New York: Appleton-Century-Crofts.

Godijn R, Theeuwes J (2003) Parallel allocation of attention prior to the execution of saccade sequences. J Exp Psychol Hum Percept Perform 29:882–896. CrossRef Medline

Goldman-Rakic PS, Schwartz ML (1982) Interdigitation of contralateral and ipsilateral columnar projections to frontal association cortex in primates. Science 216:755–757. CrossRef Medline

Heide W, Kömpf D (1998) Combined deficits of saccades and visuo-spatial orientation after cortical lesions. Exp Brain Res 123:164–171. CrossRef Medline

Histed MH, Miller EK (2006) Microstimulation of frontal cortex can reorder a remembered spatial sequence. PLoS Biol 4:e134. CrossRef Medline

Holt JL, Delvenne JF (2014) A bilateral advantage in controlling access to visual short-term memory. Exp Psychol 61:127–133. CrossRef Medline

Holtzman JD (1984) Interactions between cortical and subcortical visual areas: evidence from human commissurotomy patients. Vision Res 24:801–813. CrossRef Medline

Holtzman JD, Gazzaniga MS (1985) Enhanced dual task performance following corpus commissurotomy in humans. Neuropsychologia 23:315–321. CrossRef Medline

Horowitz TS, Wolfe JM, Alvarez GA, Cohen MA, Kuzmova YI (2009) The speed of free will. Q J Exp Psychol (Hove) 62:2262–2288. CrossRef Medline

Hudson C, Howe PD, Little DR (2012) Hemifield effects in multiple identity tracking. PLoS One 7:e43796. CrossRef Medline

Ipata AE, Gee AL, Gottlieb J, Bisley JW, Goldberg ME (2006) LIP responses to a popout stimulus are reduced if it is overtly ignored. Nat Neurosci 9:1071–1076. CrossRef Medline

Kadohisa M, Petrov P, Stokes M, Sigala N, Buckley M, Gaffan D, Kusunoki M, Duncan J (2013) Dynamic construction of a coherent attentional state in a prefrontal cell population. Neuron 80:235–246. CrossRef Medline

Kahneman D, Treisman A, Gibbs BJ (1992) The reviewing of object files:

object-specific integration of information. Cogn Psychol 24:175–219. CrossRef Medline

Kane MJ, Engle RW (2002) The role of prefrontal cortex in working-memory capacity, executive attention, and general fluid intelligence: an individual-differences perspective. Psychon Bull Rev 9:637–671. CrossRef Medline

Koffka K (1935) Principles of gestalt psychology. London: K. Paul, Trench.

Kraft A, Müller NG, Hagendorf H, Schira MM, Dick S, Fendrich RM, Brandt SA (2005) Interactions between task difficulty and hemispheric distribution of attended locations: implications for the splitting attention debate. Brain Res Cogn Brain Res 24:19–32. CrossRef Medline

Lennert T, Martinez-Trujillo JC (2013) Prefrontal neurons of opposite spatial preference display distinct target selection dynamics. J Neurosci 33: 9520–9529. CrossRef Medline

Luck SJ, Hillyard SA, Mangun GR, Gazzaniga MS (1989) Independent hemispheric attentional systems mediate visual search in split-brain patients. Nature 342:543–545. CrossRef Medline

Marino J, Schummers J, Lyon DC, Schwabe L, Beck O, Wiesing P, Obermayer K, Sur M (2005) Invariant computations in local cortical networks with balanced excitation and inhibition. Nat Neurosci 8:194–201. CrossRef Medline

Marois R, Ivanoff J (2005) Capacity limits of information processing in the brain. Trends Cogn Sci 9:296–305. CrossRef Medline

Matsushima A, Tanaka M (2012) Neuronal correlates of multiple top-down signals during covert tracking of moving objects in macaque prefrontal cortex. J Cogn Neurosci 24:2043–2056. CrossRef Medline

Matsushima A, Tanaka M (2014a) Manipulation of object choice by electrical microstimulation in macaque frontal eye fields. Cereb Cortex 24: 1493–1501. CrossRef Medline

Matsushima A, Tanaka M (2014b) Different neuronal computations of spatial working memory for multiple locations within versus across visual hemifields. J Neurosci 34:5621–5626. CrossRef Medline

Merola JL, Liederman J (1990) The effect of task difficulty upon the extent to which performance benefits from between-hemisphere division of inputs. Int J Neurosci 51:35–44. CrossRef Medline

Mitchell JF, Sundberg KA, Reynolds JH (2007) Differential attention-dependent response modulation across cell classes in macaque visual area V4. Neuron 55:131–141. CrossRef Medline

Myers RE, Sperry RW (1958) Interhemispheric communication through the corpus callosum: mnemonic carry-over between the hemispheres. AMA Arch Neurol Psychiatry 80:298–303. CrossRef Medline

Niebergall R, Khayat PS, Treue S, Martinez-Trujillo JC (2011a) Expansion of MT neurons excitatory receptive fields during covert attentive tracking. J Neurosci 31:15499–15510. CrossRef Medline

Niebergall R, Khayat PS, Treue S, Martinez-Trujillo JC (2011b) Multifocal attention filters targets from distracters within and beyond primate MT neurons' receptive field boundaries. Neuron 72:1067–1079. CrossRef Medline

Pylyshyn Z (1989) The role of location indexes in spatial perception: a sketch of the FINST spatial-index model. Cognition 32:65–97. CrossRef Medline

Pylyshyn ZW, Storm RW (1988) Tracking multiple independent targets: evidence for a parallel tracking mechanism. Spat Vis 3:179–197. CrossRef Medline

Rainer G, Asaad WF, Miller EK (1998) Memory fields of neurons in the primate prefrontal cortex. Proc Natl Acad Sci U S A 95:15008–15013. CrossRef Medline

Rao SG, Williams GV, Goldman-Rakic PS (1999) Isodirectional tuning of adjacent interneurons and pyramidal cells during working memory: evidence for microcolumnar organization in PFC. J Neurophysiol 81:1903–1916. Medline

Rizzolatti G, Riggio L, Dascola I, Umiltá C (1987) Reorienting attention across the horizontal and vertical meridians: evidence in favor of a premotor theory of attention. Neuropsychologia 25:31–40. CrossRef Medline

Scalf PE, Banich MT, Kramer AF, Narechania K, Simon CD (2007) Double take: parallel processing by the cerebral hemispheres reduces attentional blink. J Exp Psychol Hum Percept Perform 33:298–329. CrossRef Medline

Sereno AB, Kosslyn SM (1991) Discrimination within and between hemifields: a new constraint on theories of attention. Neuropsychologia 29: 659–675. CrossRef Medline

Sergent J (1990) Furtive incursions into bicameral minds: integrative and coordinating role of subcortical structures. Brain 113:537–568. CrossRef Medline

Tanaka M (2005) Involvement of the central thalamus in the control of smooth pursuit eye movements. J Neurosci 25:5866–5876. CrossRef Medline

Townsend JT (1990) Serial vs. parallel processing: sometimes they look like tweedledum and tweedledee but they can (and should) be distinguished. Psychol Sci 1:46–54. CrossRef

Treisman AM, Gelade G (1980) A feature-integration theory of attention. Cogn Psychol 12:97–136. CrossRef Medline

Wolfe JM (1994) Guided search 2.0 a revised model of visual search. Psychon Bull Rev 1:202–238. CrossRef Medline

Yantis S (1992) Multielement visual tracking: attention and perceptual organization. Cogn Psychol 24:295–340. CrossRef Medline

Hepatology Research

Hepatology Research 2014; 44: 1253–1258 doi: 10.1111/hepr.12292

Case Report

Case of presymptomatic aceruloplasminemia treated with deferasirox

Mayumi Tai,[1,2] Nobuo Matsuhashi,[1] Osamu Ichii,[1] Tomohiro Suzuki,[1] Yutaka Ejiri,[1] Satoshi Kono,[3] Tatsuhiro Terada,[3] Hiroaki Miyajima[3] and Masaru Harada[2]

[1]*Department of Gastroenterology, Fukushima Rosai Hospital, Iwaki,* [2]*The Third Department of Internal Medicine, University of Occupational and Environmental Health, Kitakyushu, and* [3]*The First Department of Medicine, Hamamatsu University School of Medicine, Hamamatsu, Japan*

Aceruloplasminemia is an autosomal recessive disease characterized by an abnormal iron metabolism. The absence of ferroxidase activity caused by mutation of ceruloplasmin leads to iron overload in the brain, liver and other organs. We report a 35-year-old man who was diagnosed with aceruloplasminemia without neurological manifestation despite the accumulation of iron in the brain and liver. To prevent the development of neurodegenerative disorder related to iron toxicity, iron depletion therapy was performed. Iron chelator deferasirox was effective in reducing serum ferritin level and to prevent the progression of the disease.

Key words: aceruloplasminemia, copper, deferasirox, iron

INTRODUCTION

ACERULOPLASMINEMIA IS AN autosomal recessive disorder caused by mutations of the ceruloplasmin gene, first reported by Miyajima *et al.* in 1987.[1] The prevalence of aceruloplasminemia was estimated to be approximately 1/2 million in non-consanguineous marriages.[2] The deficiency of ceruloplasmin results in iron overload in the brain, pancreas, liver, retina and other organs. This iron metabolic disorder is associated with the ferroxidase activity of ceruloplasmin, which is related to the oxidation of Fe^{2+} to Fe^{3+}, allowing it to be transported by transferrin.[3] Ceruloplasmin is associated with ferroportin. Ferroportin exports iron from the cells and ceruloplasmin stabilizes ferroportin in the plasma membrane of various types of cells.[4] The expression of ferroportin in the plasma membrane is regulated by hepcidin. Hepcidin is the principal regulator of systemic iron metabolism. Without ceruloplasmin or high hepcidinemia, ferroportin is internalized and degraded in the lysosomes.[5–7] Therefore, iron accumulates in various cells in patients with aceruloplasminemia.[8] Clinically, diabetes mellitus, retinal degeneration, neurological dysfunction, anemia, low serum iron and increased serum ferritin are typical features of this disease. Regarding the treatment of patients with aceruloplasminemia, several therapeutic opinions, such as iron chelation therapy, have been reported with different outcomes.[9–12]

We report a relatively young patient with aceruloplasminemia without neurological dysfunction treated with deferasirox.

CASE REPORT

A 35-YEAR-OLD MAN was diagnosed with osteomyelitis of the lower limbs and antibiotic therapy had been continued for 2 months at our orthopedics unit. At the time of admission, liver function test was normal. Abnormal liver function was detected at 1 month after the admission and drug-induced liver injury was suspected. After the cessation of antibiotics, liver dysfunction had been improved. Then, he was introduced to our unit. He had been diagnosed with anemia and insulin-dependent diabetes mellitus at the age of 16 years. There was no family history of diabetes mellitus and no medical history except his father. His father

Correspondence: Dr Mayumi Tai, Department of Gastroenterology, Fukushima Rosai Hospital, 3 Numaziri Tsuzuramachi, Uchigo Iwaki City, Fukushima 973-8403, Japan. Email: tai-mayu@fukushima-rosai.jp

Received 16 July 2013; revision 5 December 2013; accepted 10 December 2013.

had presented with Parkinson's disease in the past several years. His parents were not consanguineous. On examination, he showed no evident neurological or ophthalmoscopic abnormalities. Kayser–Fleischer ring was not detected. Laboratory data at admission to our unit is shown in Table 1. They include increased serum ferritin (3530 ng/dL), low serum copper concentration (9 μg/dL), undetectable ceruloplasmin (<1.0 g/dL), hepcidin-25 (<0.7 ng/mL) and normal urinary copper excretion (35 μg/L).

Abdominal computed tomography (CT) showed a high density of the liver. T_1- and T_2-weighted brain magnetic resonance imaging (MRI) showed an abnormal hypointensity in the basal ganglia, hypothalamus and dentate nucleus, suggesting the accumulation of iron in these regions (Fig. 1). A liver biopsy showed almost normal architecture, however, severe iron accumulation was demonstrated in hepatocytes and Kupffer cells. Copper staining was negative by rubeanic acid staining (Fig. 2). After informed consent was obtained, the genomic analysis of the ceruloplasmin gene was performed, which revealed a homozygous mutation at the nucleotide in exon 16, causing a missense Gly→Glu substitution at position 873 (G873E) (Fig. 3). This mutation has not been described previously. The analysis of *ATP7B* did not reveal mutations related to Wilson's disease and the analysis of *HFE*, *HJV*, *HAMP*, *TFR2* and *SLC40A1* did not reveal mutations related to iron overload. We diagnosed the patient with aceruloplasminemia. To prevent the development of neurological dysfunction, iron chelating therapy with an oral iron chelating agent (deferasirox) was performed. The initial dose of deferasirox (500 mg/day) was administrated for 6 months but serum ferritin concentration did not decrease. We increased the dose of deferasirox to 1000 mg/day. At 5 months after the increase of the dose, serum ferritin level decreased from 952 to 250 ng/dL without any side-effects. Then, we decreased the dose of deferasirox to 500 mg/day and the serum ferritin level continued within the normal range (Fig. 4). The patient tolerated the therapy without any side-effects. However, his glycemic control was not improved and the abnormal hypointensity of the brain MRI was almost unchanged compared to the first MRI (Fig. 1).

Table 1 Laboratory findings of the present patient

Complete blood counts	
White blood cells	5700/μL
Red blood cells	347×10^4/μL
Hb	9.5 g/dL
Ht	30.9%
MCV	89 fl
MCH	27 pg
Plt	21×10^4/μL
Coagulation	
PT	128%
INR	0.88
APTT	29 s
Biochemistry	
TP	7.2 g/dL
Alb	4.44 g/dL
T-bil	0.37 mg/dL
AST	59 IU/L
ALT	106 IU/L
LDH	218 IU/L
ALP	434 IU/L
γ-GT	35 IU/L
Ch-E	252 IU/L
BUN	27.4 mg/dL
Cre	0.5 mg/dL
Na	138 mEq/L
K	5.08 mEq/L
Cl	102.8 mEq/L
T-cho	150 mg/dL
CRP	0.03 mg/d
Ferritin	3530 ng/mL
TIBC	282 μg/dL
Fe	46 μg/dL
Cu	9 μg/dL
Ceruloplasmin	<1.0 mg/dL
Hepcidin-25	<0.7 ng/mL
Immunology	
ANA	<40
AMA 2	<5
Viral marker	
HBsAg	(−)
HCV Ab	(−)
Urinalysis	
U-Cu	35 μg/L
U-Cr	284.5 mg/dL

Ab, antibody; Alb, albumin; ALP, alkaline phosphatase; ALT, alanine aminotransferase; AMA2, antimitochondrial antibody 2; ANA, antinuclear antibody; APTT, activated partial thromboplastin time; AST, aspartate aminotransferase; BUN, blood urea nitrogen; Ch-E, cholinesterase; Cre, creatinine; CRP, C-reactive protein; Hb, hemoglobin; HBsAg, hepatitis B surface antigen; HCV, hepatitis C virus; Ht, hematocrit; INR, International Normalized Ratio; LDH, lactate dehydrogenase; MCH, mean corpuscular hemoglobin; MCV, mean corpuscular volume; Plt, platelets; PT, prothrombin time; T-bil, total bilirubin; T-cho, total cholesterol; TIBC, total iron binding capacity; TP, total protein; U, urinary excretion; γ-GT, γ-glutamyltransferase.

DISCUSSION

CERULOPLASMIN PLAYS AN important role in the iron metabolism and scavenges the H_2O_2; its deficiency results in oxidative stress with iron overload in the brain.[13] In many cases of aceruloplasminemia, the

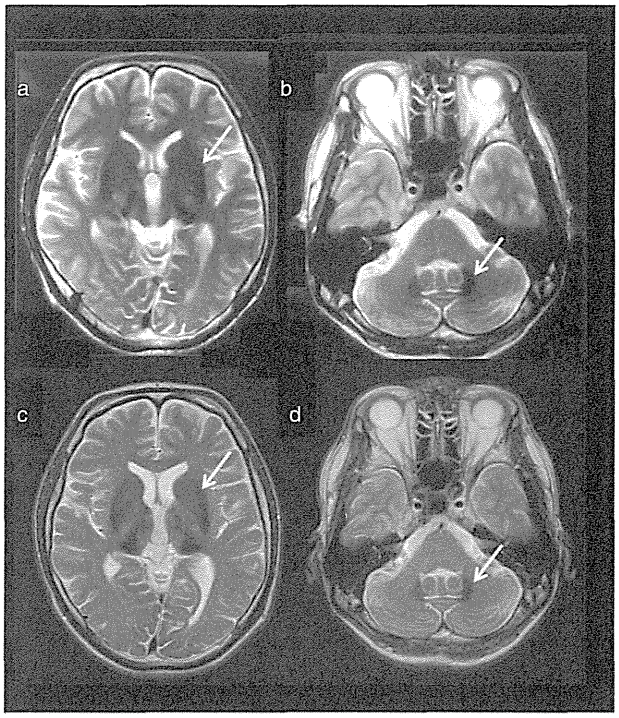

Figure 1 Magnetic resonance imaging (MRI) of the brain. Comparative study of T_2-weighted axial image (a,b) before and (c,d) 2 years after the treatment with deferasirox. MRI showed low signal intensity in the basal ganglia (arrows) and hypothalamus (arrows) (a) before and (c) after the treatment. MRI showed low signal intensity in the dentate nucleus (arrows) (b) before and (d) after the treatment.

neurological abnormality caused by iron deposition is the first manifestation. In our case, we found decreased serum ceruloplasmin and low plasma copper in the examination for the cause of liver dysfunction and Wilson's disease was suspected. However, the lack of increased urinary copper excretion did not suggest Wilson's disease. The characteristic MRI findings, normal serum iron and increasing plasma ferritin led to the suspicion of aceruloplasminemia. To confirm the diagnosis, we performed the genetic analysis of the ceruloplasmin, Wilson's disease and some types of hereditary hemochromatosis. The ceruloplasmin gene is composed of 20 exons and located in chromosome 3q25. More than 40 mutations in the ceruloplasmin gene have been recognized due to the Human Gene Mutation Database (http://www.hgmd.cf.ac.uk/ac/index.php). In our case, G at nucleotide 2679 to A transversion was detected in the exon 16 which changed Gly at codon 873 to Glu. This mutation has not been described previously. Many mutations are reported in patients with aceruloplasminemia, however, there is no genotype–phenotype correlation.[14,15] Wilson's disease is associated with genetic defects in *ATP7B*, which is associated with low ceruloplasminemia.

In our case, the mutation associated with copper overload in *ATP7B* was not found and low hepcidinemia was apparent. Mutations in the hereditary hemochromatosis gene and aceruloplasminemia provide low or deficiency of serum hepcidin.[6,7] In our case, the hemochromatosis gene mutation (*HFE*, *HJV*, *HAMP*, *TFR2* and *SLC40A1*) associated with iron overload was not found. Kono *et al.* identified that the mutant ceruloplas-

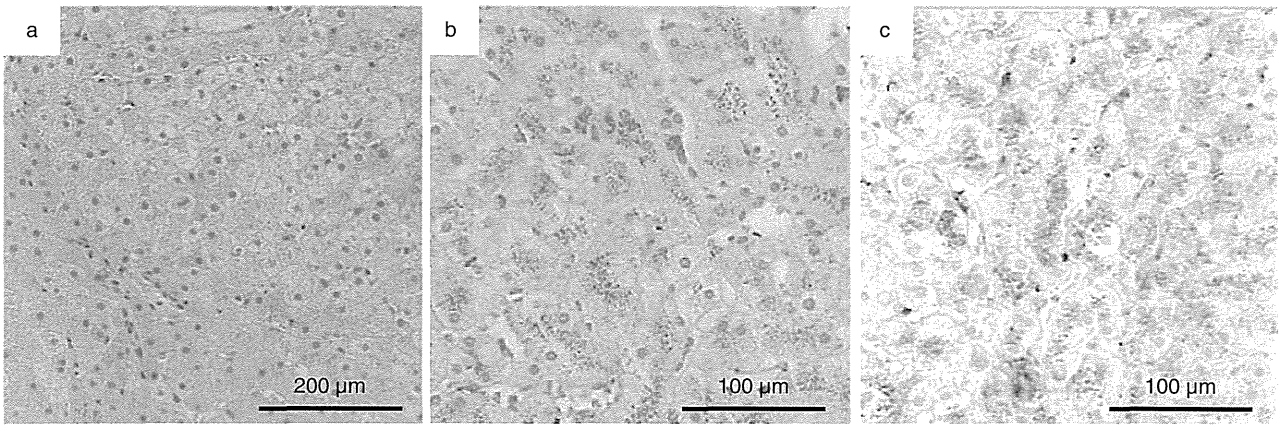

Figure 2 Histological analysis of the liver biopsy specimen. (a) Hematoxylin–eosin staining. Fibrosis and cirrhosis was not observed (original magnification ×20). (b) Rubeanic acid staining. Copper binding protein was negative in hepatocytes (×40). (c) Berlin blue staining. Severe iron staining was observed in hepatocytes and Kupffer cells (×40).

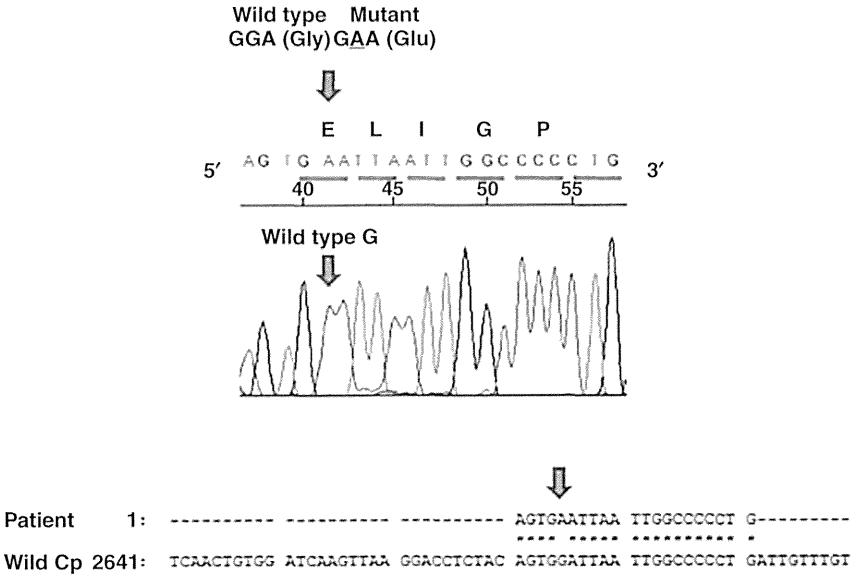

Figure 3 Sequence analysis of ceruloplasmin gene exon 16. Arrow indicates the mutation that substitutes from Gly to Glu.

min was associated with decreased ferroxidase activity resulting in loss of ferroportin stability under low levels of hepcidin.[6] In our case, the liver dysfunction was improved after the cessation of antibiotics without iron chelation. Therefore, it seemed that the liver dysfunction was caused by drugs. Because the liver injury was mild, it seemed that the extremely high serum ferritin level on admission was affected by inflammation of osteomyelitis. Neither functional disturbance nor necrosis was shown in the liver of aceruloplasminemia despite massive iron deposition.[13,16–18] In the present case, copper binding protein was negative in hepatocytes and the red-brown granular material was iron (Fig. 2b,c). Severe iron accumulation in hepatocytes was observed,

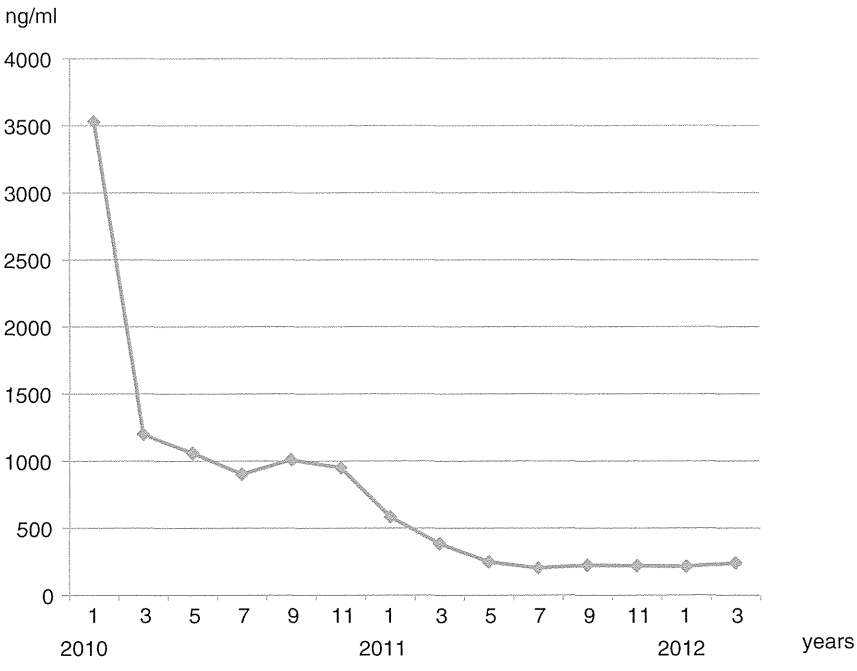

Figure 4 Change of the serum ferritin concentration.

however, few inflammatory cells were observed (Fig. 2c).

It is hypothesized that the difference in tissue injury between the brain and the liver is due to the many antioxidant enzymes in the liver.[13] In fact, the activity of catalase in the liver is more than 30-times higher than that in the brain.[19] In the present case, the first clinical manifestation was adult-onset diabetes mellitus, but retinal degeneration was not present. The neurological disease might have appeared several years later, if he had not been treated.

Iron chelating therapy for aceruloplasminemia has been reported, but the clinical efficacy of the patient has varied. In the present case, the treatment with deferasirox led to a reduction of serum ferritin, but the hepatic deposition analyzed by CT scan did not change. In some cases, brain MRI showed a steady hyposignal of the iron deposition even after the treatment, despite a decrease of hepatic iron accumulation and serum ferritin.[9,20,21] These data suggest that iron chelating therapy may be useful in limiting the liver iron deposition but not in brain iron deposition. In another case, the treatment with desferrioxamine led to a reduction of serum ferritin and neurological abnormalities as well as the improvement of diabetes.[11] A case of aceruloplasminemia with neurological symptoms despite visible iron deposition on the brain MRI was reported, in which deferasirox therapy improved neurological symptoms.[22] Deferasirox was effective in another case with neurological symptoms.[23] Therefore, early diagnosis and treatment must be important and the iron removal therapy may be effective to prevent the development of neurological dysfunction. Because it was reported that several side-effects prohibit the long-term treatment with deferasirox, it is important to monitor anemia and renal dysfunction and clinical symptoms, particularly gastrointestinal disturbances and skin rashes, when iron chelating therapy with deferasirox is continued.[21,24,25]

In conclusion, we report a case with aceruloplasminemia in whom iron chelating therapy using deferasirox was useful to reduce serum ferritin concentration and to prevent progression of the phenotype.

ACKNOWLEDGMENT

WE THANK DR Hisao Hayashi (Aichi Gakuin University, School Of Pharmacy) for the genetic analysis of Wilson's disease and the hereditary hemochromatosis genes.

REFERENCES

1 Miyajima H, Nishimura Y, Mizoguchi K *et al.* Familial apoceruloplasmin deficiency associated with blepharospasm and retinal degeneration. *Neurology* 1987; **37:** 761–7.
2 Miyajima H, Kohno S, Takahashi Y *et al.* Estimation of the gene frequency of aceruloplasminemia in Japan. *Neurology* 1999; **53:** 617–9.
3 Osaki S, Johnson DA, Frieden E. The possible significance of the ferrous oxidase activity of ceruloplasmin in normal human serum. *J Biol Chem* 1966; **241:** 2746–51.
4 De Domenico I, Ward DM, di Patti MC *et al.* Ferroxidase activity is required for the stability of cell surface ferroportin in cells expressing GPI-ceruloplasmin. *EMBO J* 2007; **26:** 2823–31.
5 Pietrangelo A. Hereditary hemochromatosis: pathogenesis, diagnosis, and treatment. *Gastroenterology* 2010; **139:** 393–408.
6 Kono S, Yoshida K, Tomosugi N *et al.* Biological effects of mutant ceruloplasmin on hepcidin-mediated internalization of ferroportin. *Biochim Biophys Acta* 2010; **1802:** 968–75.
7 Kaneko Y, Miyajima H, Pipemo A *et al.* Measurement of serum hepcidin-25 levels as a potential test for diagnosing hemochromatosis and related disorders. *J Gastroenterol* 2010; **45:** 1163–71.
8 Harris ZL, Klomp LW, Gitlin JD. Aceruloplasminemia: an inherited neurodegenerative disease with impairment of iron homeostasis. *Am J Clin Nutr* 1998; **67:** 972S–7S.
9 Lorēal O, Turlin B, Pigeon C *et al.* Aceruloplasminemia: new clinical, pathophysiological and therapeutic insights. *J Hepatol* 2002; **36:** 851–6.
10 Mariani R, Arosio C, Pelucchi S *et al.* Iron chelation therapy in aceruloplasminemia: study of a patient with a novel missense mutation. *Gut* 2004; **53:** 756–8.
11 Miyajima H, Takahashi Y, Kamata T *et al.* Use of desferrioxamine in the treatment of aceruloplasminemia. *Ann Neurol* 1997; **41:** 404–7.
12 Yonekawa M, Okabe T, Asamoto Y *et al.* A case of hereditary ceruloplasmin deficiency with iron deposition in the brain associated with chorea, dementia, diabetes mellitus and retinal pigmentation: administration of fresh-frozen human plasma. *Eur Neurol* 1999; **42:** 157–62.
13 Tajima K, Kawanami T, Nagai R *et al.* Hereditary ceruloplasmin deficiency increases advanced glycation end products in the brain. *Neurology* 1999; **53:** 619–22.
14 Yoshida K. Mutations in the ceruloplasmin gene in aceruloplasminemia. *Neurol Med* 2004; **61:** 146–50. (In Japanese.)
15 Yoshida K, Kaneko K. Aceruloplasminemia. *Neurol Med* 2009; **71:** 517–26. (In Japanese.)
16 Kawanami T, Kato T, Daimon M *et al.* Hereditary ceruloplasmin deficiency: clinicopathological study of a patient. *J Neurol Neurosurg Psychiatry* 1996; **61:** 506–9.
17 Wada S, Kimura K, Mizuno I *et al.* A case of aceruloplasminemia associated with insulin-dependent diabetes

mellitus, cerebellar ataxia and retinal degeneration. *Folia Endocrinol* 1996; 72: 543–50. (In Japanese.)
18 Daimon M. Hereditary ceruloplasmin deficiency. *Nippon Rinsho* 2008; 66: 563–67. (In Japanese.)
19 Tiedge M, Lortz S, Drinkgern J *et al.* Relation between antioxidant enzyme expression and antioxidative defense status of insulin-producing cells. *Diabetes* 1997; 46: 1733–42.
20 Fasano A, Colosimo C, Miyajima H *et al.* Aceruloplasminemia: a novel mutation in a family with marked phenotypic variability. *Mov Disord* 2008; 23: 751–5.
21 Finkenstedt A, Wolf E, Höfner E *et al.* Hepatic but not brain iron is rapidly chelated by deferasirox in aceruloplasminemia due to a novel gene mutation. *J Hepatol* 2010; 53: 1101–7.
22 Skidmore FM, Dragon V, Foster P *et al.* Aceruloplasminemia with progressive atrophy without brain iron overload: treatment with oral chelation. *J Neurol Neurosurg Psychiatry* 2008; 79: 467–70.
23 McNeill A, Pandolfo M, Kuhn J *et al.* The neurological presentation of ceruloplasmin gene mutations. *Eur Neurol* 2008; 60: 200–5.
24 Suzuki Y, Yoshida K, Aburakawa Y *et al.* Effectiveness of oral iron chelator treatment with Deferasirox in an aceruloplasminemia patient with a novel ceruloplasmin gene mutation. *Intern Med* 2013; 52: 1527–30.
25 Lee JW. Iron chelation therapy in the myelodysplastic syndromes and aplastic anemia: a review of experience in South Korea. *Int J Hematol* 2008; 88: 16–23.

NEUROPATHOLOGY

Neuropathology 2015; **35**, 83–90 doi:10.1111/neup.12149

Symposium: Neurodegeneration with Brain Iron Accumulation

Aceruloplasminemia

Hiroaki Miyajima

First Department of Medicine, Hamamatsu University School of Medicine, Hamamatsu, Japan

Aceruloplasminemia is characterized by progressive neurodegeneration with brain iron accumulation due to the complete lack of ceruloplasmin ferroxidase activity caused by mutations in the ceruloplasmin gene. Redox-active iron accumulation was found to be more prominent in the astrocytes than in the neurons. The most characteristic findings were abnormal or deformed astrocytes and globular structures of astrocytes. The lack of ceruloplasmin may primarily damage astrocytes in the aceruloplasminemic brains as a result of lipid peroxidation due to massive iron deposition. In the normal brain, iron may be continuously recycled between astrocytes and neurons, with transferrin acting as a shuttle. The glycosylphosphatidylinositol (GPI)-linked ceruloplasmin on astrocytes functions as a ferroxidase, mediating the oxidation of ferrous iron transported from the cytosol by ferroportin and its subsequent transfer to transferrin. In cases with aceruloplasminemia, neurons take up the iron from alternative sources of non-transferrin-bound iron, because astrocytes without GPI-linked ceruloplasmin cannot transport iron to transferrin. The excess iron in astrocytes could result in oxidative damage to these cells, and the neuronal cell protection offered by astrocytes would thus be disrupted. Neuronal cell loss may result from iron starvation in the early stage and from iron-mediated oxidation in the late stage. Ceruloplasmin may therefore play an essential role in neuronal survival in the central nervous system.

Key words: ceruloplasmin, iron, ferroxidase, ferroportin, hepcidin, neurodegeneration, iron metabolic cycle.

INTRODUCTION

Iron is an essential bioactive metal that participates in a variety of brain functions, including the biosynthesis of neurotransmitters, myelin formation and energy metabolism. On the other hand, excessive iron in the brain causes neuronal injury and cell death, because redox-active ferrous iron (Fe^{2+}) enhances oxidative stress via the generation of the highly cytotoxic hydroxyl radical. However, the precise mechanisms of iron metabolism and regulation in the brain remain unknown.

In 1987, we described the first case of aceruloplasminemia in a 52-year-old Japanese female suffering from blepharospasm, retinal degeneration and diabetes mellitus (DM).[1] Subsequent evaluations revealed the presence of anemia and low serum iron concentrations, despite high levels of serum ferritin and marked iron accumulation in the brain and visceral organs, as well as a complete absence of serum ceruloplasmin. The patient was homozygous for a five base insertion in exon 7 in the ceruloplasmin gene.[2] The novel disorder was thus termed aceruloplasminemia (MIM 604290). Clinical and pathological studies in patients with aceruloplasminemia and ceruloplasmin knockout mice revealed that there was increased lipid peroxidation due to iron-mediated cellular radical injury caused by massive iron accumulation.[3] In the following review of aceruloplasminemia, the functions of ceruloplasmin will be presented, and the role of ceruloplasmin in brain iron metabolism will be discussed.

Ceruloplasmin

Ceruloplasmin is a blue copper oxidase and contains 95% of the copper present in human serum. It is initially synthesized as an apo-protein, which binds up to six atoms of copper, and then changes to a holo-form (called ceruloplasmin).[4] There are two isoforms of this protein generated by alternative splicing, a secretory form (serum ceruloplasmin) and a glycosylphosphatidylinositol (GPI)-linked form.[5] The secretory form is expressed only in hepatocytes, while the GPI-linked form is expressed in the brain, liver, lungs, kidneys and several other organs.[6] The secretory ceruloplasmin plays a role as a NO oxidase that determines endocrine NO homeostasis,[7] and is upregulated as an acute phase protein by inflammation, trauma and

Correspondence: Hiroaki Miyajima, MD, First Department of Medicine, Hamamatsu University School of Medicine, 1-20-1 Handayama, Higashi-ku, Hamamatsu 431-3192, Japan. E-mail, miyajima@hama-med.ac.jp

Received 9 July 2014; revised and accepted 22 July 2014; published online 28 August 2014.

pregnancy, which is attributed to its properties as an antioxidant.[8] The GPI-linked form anchors to the cell membranes of various tissues and plays a role in iron efflux from cells as a ferroxidase.[9]

Aceruloplasminemia revealed the essential role for ceruloplasmin in brain iron homeostasis. Serum ceruloplasmin does not cross the blood-brain barrier in the normal brain. Instead, GPI-linked ceruloplasmin is bound to the cell membranes of astrocytes, where it plays an important role in iron efflux from astrocytes due to the activity of ferroxidase, which oxidizes ferrous iron following its transfer to the cell surface via ferroportin, and delivers ferric iron to extracellular transferrin (Fig. 1). Ferroportin is post-translationally regulated through internalization triggered by hepcidin binding.[10] Hepcidin is synthesized by astrocytes and microglia, as well as the hepatocytes. The prevention of hepcidin-mediated ferroportin internalization was observed in glioma cells lines expressing endogenous ceruloplasmin, as well as in the cells transfected with GPI-linked ceruloplasmin under low levels of hepcidin.[11] A decrease in the extracellular level of ferrous iron by an iron chelator and by incubation with purified ceruloplasmin in the culture medium prevented hepcidin-mediated ferroportin internalization, while the reconstitution of apo-ceruloplasmin was not able to prevent ferroportin internalization. Mutant ceruloplasmin cannot stabilize ferroportin because of the loss-of-function in the ferroxidase activity, which has been reported to play an important role in the stability of ferroportin.[12]

It is now known that (i) ceruloplasmin regulates the efficiency of iron efflux, (ii) ceruloplasmin functions as a ferroxidase and regulates the oxidation of ferrous iron (Fe^{2+}) to ferric iron (Fe^{3+}), (iii) ceruloplasmin does not bind to transferrin directly, (iv) ceruloplasmin stabilizes the cell surface iron transporter, ferroportin and (v) GPI-linked ceruloplasmin is the predominant form expressed in the brain.[6] The ceruloplasmin-ferroportin system represents the main pathway for cellular iron egress, and it is responsible for the physiological regulation of the cellular iron levels.

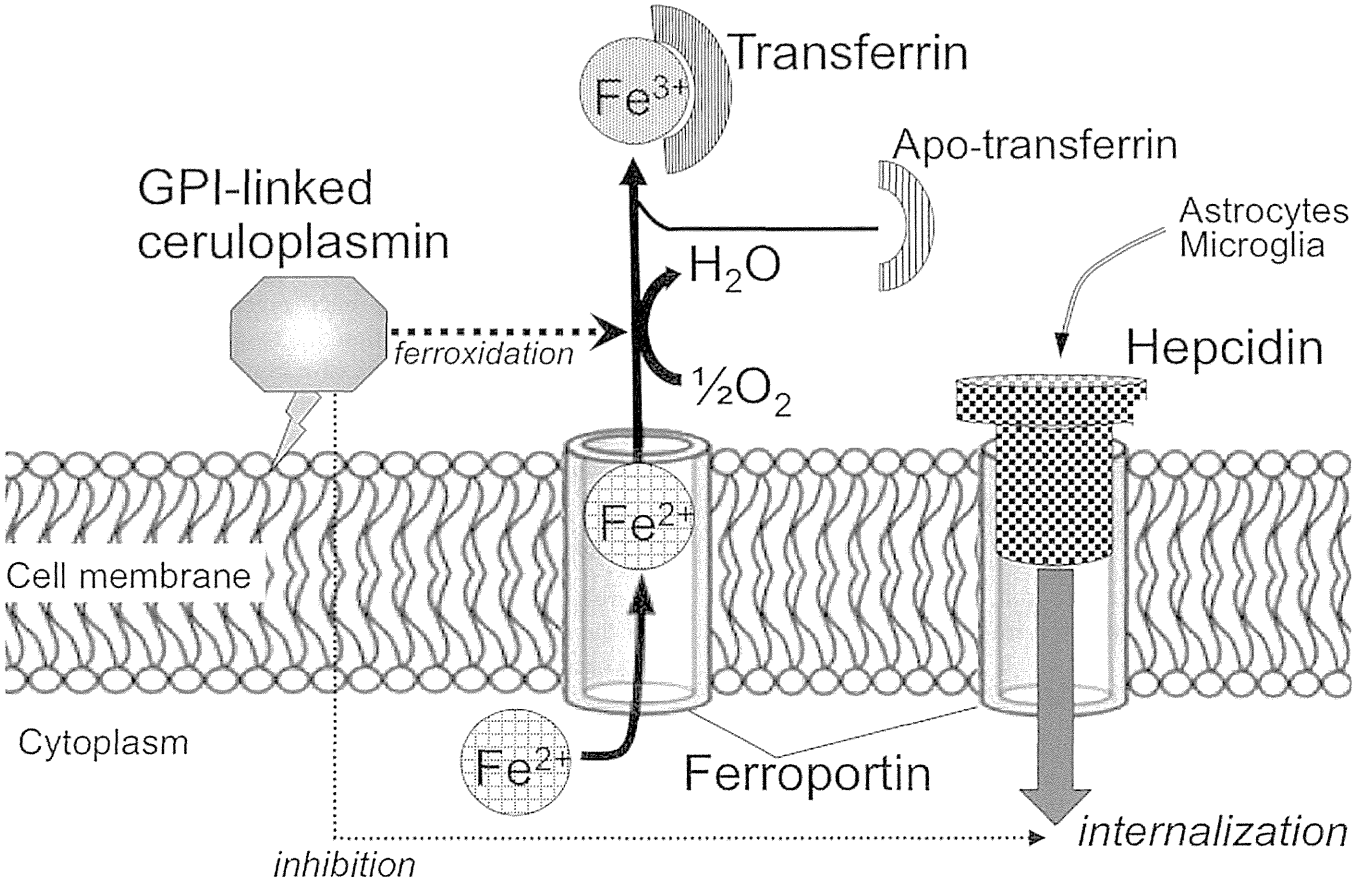

Fig. 1 Iron transport at the cell membrane of the astrocytes. An iron transporter, ferroportin, transports intracellular ferrous iron (Fe^{2+}) to extracellular transferrin. Ceruloplasmin functions as a ferroxidase converting ferrous iron (Fe^{2+}) to ferric iron (Fe^{3+}). Ferric iron binds directly to apo-transferrin. Ceruloplasmin regulates the efficiency of iron efflux. It also inhibits the ferroportin internalization triggered by hepcidin binding.